JOURNAL OF PETROLOGY | VOLUME 47 | NUMBER 3 | PAGES 457–479 | 2006 | doi:10.1093/petrology/egi082

A 2.5 ka History of Dacitic Magmatism at Nevado de Toluca, Mexico: Petrological, $^{40}Ar/^{39}Ar$ Dating, and Experimental Constraints on Petrogenesis

J. L. ARCE[1]*, J. L. MACIAS[2], J. E. GARDNER[3] AND P. W. LAYER[4]

[1]INSTITUTO DE GEOLOGIA, UNAM, COYOACÁN 04510, MÉXICO D.F., MEXICO

[2]INSTITUTO DE GEOFÍSICA, UNAM, COYOACÁN 04510, MÉXICO D.F., MEXICO

[3]DEPARTMENT OF GEOLOGICAL SCIENCES, UNIVERSITY OF TEXAS, AUSTIN, TX 78712-0254, USA

[4]GEOPHYSICAL INSTITUTE AND DEPARTMENT OF GEOLOGY AND GEOPHYSICS, UNIVERSITY OF ALASKA, FAIRBANKS, AK 99775-7320, USA

RECEIVED AUGUST 27, 2003; ACCEPTED SEPTEMBER 29, 2005
ADVANCE ACCESS PUBLICATION NOVEMBER 7, 2005

After 11·5 ka of quiescence (24·5–13 ka), the Nevado de Toluca volcano started a 2500 year period of activity. This period was characterized by a dome destruction event at 13 ka, a small Plinian event at 12·1 ka, and a large Plinian eruption at 10·5 ka. About 10 km^3 of magma was erupted that was homogeneous in composition (63·3–65·7 SiO_2 wt % whole-rock) and in mineralogy. Pumice consists of plagioclase ($An_{30–59}$) > orthopyroxene ($En_{56–59}$) > hornblende ≫ Fe–Ti oxides + rare apatite (in opx) + biotite, set in a rhyolitic matrix (72–76 SiO_2 wt %). $^{40}Ar/^{39}Ar$ analysis of single biotite crystals yielded ages (0·81–4·7 Ma), that do not correspond to eruption ages. The biotite represents partially assimilated xenocrysts, which could have resided in the magma for only a short period of time. Mineral chemical data, coupled with hydrothermal experiments, indicate that prior to eruption the dacitic magma stagnated at a depth of 4·5–6 km below the summit at water pressures of 160–210 MPa and a temperature of 824 ± 12°C on the basis of Fe–Ti oxide thermometry, and under water-saturated conditions. To stabilize a homogeneous magma body of >10 km^3 at 824°C in the upper crust, we propose that reheating of the dacitic reservoir by hotter magma batches was able to maintain the equilibrium between the temperature of the magma and the assimilation of wall-rock over a period of 2500 years. Based on similarities among the juvenile products, we suggest that the three eruptions were fed from the same magma body.

KEY WORDS: *explosive volcanism; xenocrystic contamination; Nevado de Toluca, Mexico*

INTRODUCTION

Nevado de Toluca is a stratovolcano [19°06′30″N; 99°45′30″W; 4680 m above sea level (a.s.l.)] located 80 km SW of Mexico City in the central part of the Trans-Mexican Volcanic Belt (Fig. 1a). Volcanic activity commenced ~2·5 Ma ago with the emplacement of andesitic lava flows, ending at about 1·3 Ma (Cantagrel *et al.*, 1981; Macías *et al.*, 1997; García-Palomo *et al.*, 2002). Renewed activity took place at about 100 ka through the emission of dacitic pyroclastic products. The most recent period of intense activity at Nevado de Toluca lasted for about 2500 years from 13 to 10·5 ka, after ~11·5 ka of quiescence, during which three pyroclastic deposits were produced by three different volcanic eruptions. Samples analyzed from these deposits are relatively homogeneous in composition and mineralogy, which raises the question of whether the three magmas were fed from a single, large reservoir or from several small magma bodies. If they originated from a single reservoir, it is interesting to consider how much change occurred in the magma during the 2500 years.

Several models have been proposed to explain the origin of dacitic rocks in volcanic systems; these include a simple crystal fractionation of basaltic or andesitic parental magmas (Berman, 1981; Reid & Cole, 1983), mixing between rhyolitic and basaltic magmas (Eichelberger, 1975; Gerlach & Grove, 1982), crustal contamination of mafic magmas (Francis *et al.*, 1980; Harmon *et al.*, 1981;

*Corresponding author. Telephone: 52-55-56224288, ext. 108. Fax: 52-55-562242889. E-mail: jlarce@geologia.unam.mx

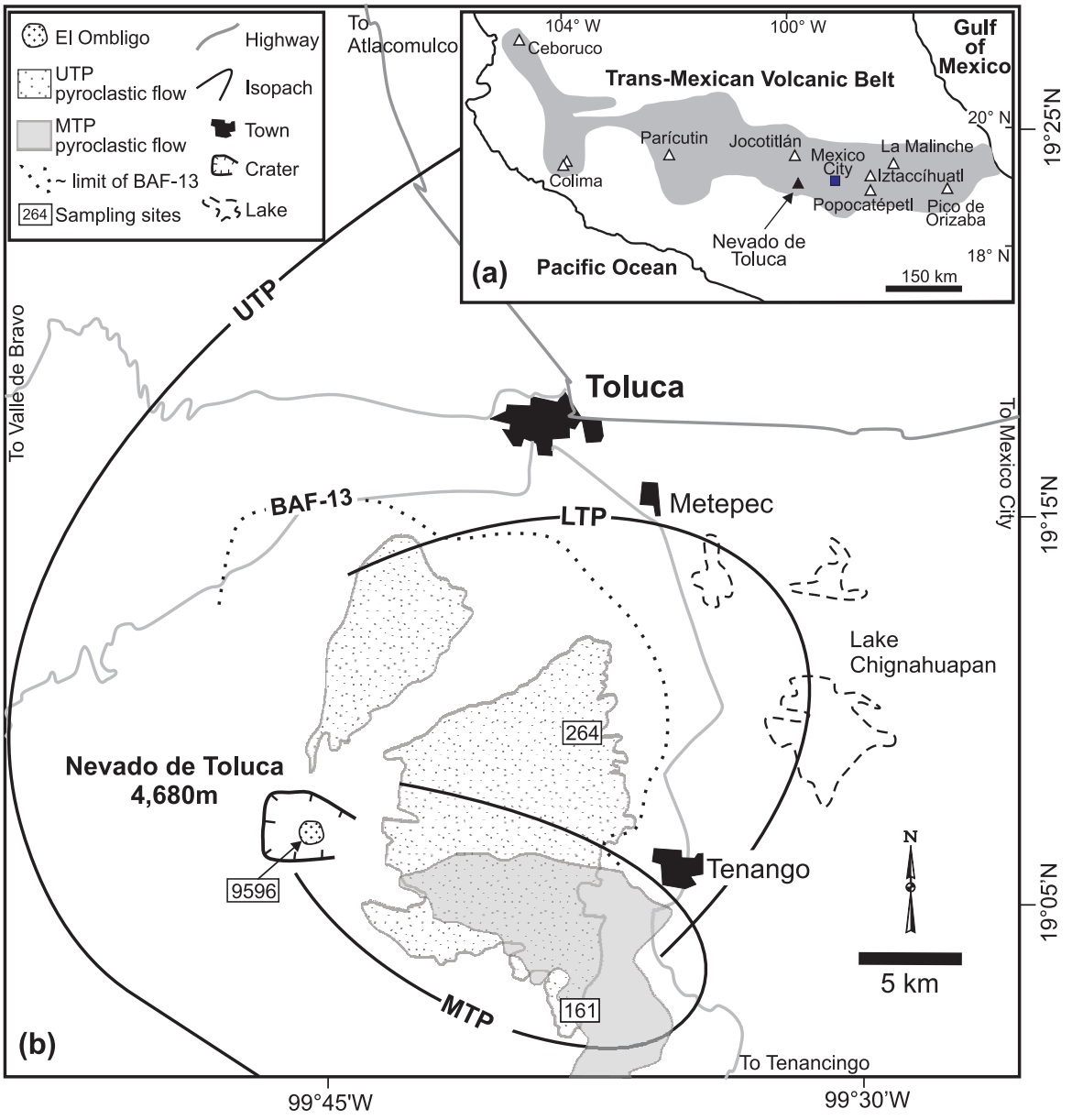

Fig. 1. (a) Location map of Nevado de Toluca volcano within the Trans-Mexican Volcanic Belt. △, some volcanoes in Mexico. (b) Map showing the distribution of the Upper Toluca Pumice (UTP), Middle Toluca Pumice (MTP), block-and-ash flow deposit of ~13 ka (BAF-13) and Lower Toluca Pumice (LTP), and the main sampling sites.

Grant *et al.*, 1984), and partial melting of the lower crust (Reid & Cole, 1983; Grant *et al.*, 1984). Recent petrological studies have suggested that silicic magmas are probably produced by a combined process of fractionation and assimilation (Hopson & Mattinson, 1990; Grove *et al.*, 1997). However, the time required to produce and store such magmas in the crust is still unclear (e.g. Hawkesworth *et al.*, 2000; Reagan *et al.*, 2003).

The recurrence of silicic volcanism can be explained by a number of models; one of these considers that the magmas are fed from a single, long-lived reservoir (Halliday *et al.*, 1989; van den Bogaard & Schirnick, 1995), whereas in another the magmas are generated by fast and repetitive partial melting of the lower crust (Huppert & Sparks, 1988; Sparks *et al.*, 1990).

The Nevado de Toluca volcano offers an opportunity to investigate the mechanism responsible for generating eruptions of three, closely spaced in time, homogeneous dacitic magmas. The results of detailed petrological studies combined with hydrothermal experiments are

used to investigate the evolution of the magmatic system during this period of its activity. All analytical methods are described in Appendix A.

SUMMARY OF THE 2500 YEARS OF ACTIVITY

The late Pleistocene stratigraphic sequence of Nevado de Toluca volcano consists of three pyroclastic deposits informally designated BAF-13 (13 ka), MTP (12·1 ka), and UTP (10·5 ka), each of which was deposited to the NE–ESE of the volcano (Fig. 1b).

Block-and-ash flow deposit 13 (BAF-13)

The BAF-13 deposit, erupted between 13 160 ± 89 years BP (before present) and 13 870 +445/–420 years BP (Caballero-Miranda *et al.*, 2001; García-Palomo *et al.* 2002), consists, from the base upward, of a grey laminated surge layer (10 cm thick), overlain by two 2 m thick, massive, grey, block-and-ash flow layers, each composed of light and dark grey dacitic blocks, grey and white dacitic pumice, and minor reddish altered blocks set in a coarse ash matrix (Fig. 2). The stratigraphy of BAF-13 suggests that a pre-existing dacitic dome in the crater was destroyed by magmatic explosions that produced pyroclastic surges and pyroclastic flows. The volume of material ejected during this volcanic event is not well constrained but its thickness and extent suggest a maximum of 0·5 km^3 dense rock equivalent (DRE).

Middle Toluca Pumice (MTP)

The Middle Toluca Pumice consists of a complex pyroclastic sequence (Fig. 2) of five fall horizons generated by a small Plinian eruption dated at 12 040 ± 95 and 12 415 ± 285 years BP (Macías *et al.*, 1997; Cervantes, 2001; García-Palomo *et al.*, 2002; Arce *et al.*, 2003). The juvenile material of the MTP deposit consists of white, grey, and banded dacitic pumice. The volume of the magma ejected during this volcanic eruption is estimated to be 1·8 km^3 (Cervantes, 2001; Arce *et al.*, 2005).

Upper Toluca Pumice (UTP)

The UTP deposit has been described by several workers (Bloomfield & Valastro, 1974; Bloomfield *et al.*, 1977; Macías *et al.*, 1997; Arce *et al.*, 2003). The UTP is a complex sequence composed of four fall horizons, four pyroclastic flow units, and two pyroclastic surge units, all erupted at 10·5 ka (Arce *et al.*, 2003) (Fig. 2). The UTP deposit contains white, grey, and banded dacitic pumice, and dense, light grey, lithic fragments. These constituents vary through the stratigraphic sequence; at the base, grey pumice and dense lithic clasts are more abundant (F0, PC0 and base of PC1 units). Stratigraphically upwards, white pumice dominates the deposit. Minor amounts of banded pumice appear throughout the stratigraphy. The volume of the magma ejected during this eruption was estimated to be ~8 km^3 (Arce *et al.*, 2003). The UTP sequence is capped by a dacitic central dome called El Ombligo, which is considered to be the last product of the UTP eruption (Arce *et al.*, 2003).

PETROGRAPHY OF THE DEPOSITS

Block-and-ash-flow deposit 13 (BAF-13)

White and grey pumice are highly porphyritic and dacitic in composition (Fig. 3), containing, in order of abundance, phenocrysts of plagioclase, orthopyroxene, hornblende, and minor Fe–Ti oxides and biotite, all set in highly vesicular glass (Fig. 4; Table 2). White pumice contains 53·54 vol. % phenocrysts, whereas grey pumice contains 46·50 vol. % (Table 1); both pumice types are relatively more crystalline than the UTP and MTP pumice (described below). We recognize two populations of crystals. The first includes large phenocrysts, all of which have resorbed margins and subhedral to anhedral shapes. The second population comprises small phenocrysts (<1 mm) that are all euhedral. All biotite crystals, regardless of size, are rimmed by reaction products. Plagioclase phenocrysts are weakly reversely zoned, with cores on average of $An_{45\pm7}$ and rims of $An_{47\pm1}$ (Table 3). Microphenocrysts are $An_{45\pm6}$. Orthopyroxene is unzoned, averaging $En_{58\cdot8\pm0\cdot3}$ (Table 4). Amphibole is edenite–pargasite hornblende. Biotite is ferroan–phlogopite, similar to that found in the UTP samples (Table 5). Ilmenite and rare titanomagnetite are present as isolated crystals in the matrix and as inclusions in the phenocrysts (biotite, orthopyroxene, and hornblende). The composition of ilmenite is Ilm 0·80 (mole fraction ilmenite) and that of titanomagnetite is Usp 0·22 (mole fraction ulvöspinel) (Table 6).

Middle Toluca Pumice

White and grey pumice from the MTP are similar in composition (Fig. 3; Table 7), but differ significantly in crystallinity (Table 1). Phenocrysts consist of plagioclase > orthopyroxene > hornblende ≫ Fe–Ti oxides + biotite, all set in a vesicular rhyolitic glass (73 wt % SiO_2) (Table 2). Larger phenocrysts (>1 mm diameter) have resorption textures; biotite crystals have reaction rims and resorbed margins (Fig. 5), whereas small phenocrysts (<1 mm diameter) are euhedral.

Plagioclase is essentially unzoned with cores ranging from $An_{45\cdot8\pm6}$ to $An_{48\pm4}$, and rims from $An_{46\cdot5\ \pm1}$ to $An_{45\pm1}$. Microphenocrysts average $An_{45\pm2}$ (Table 3). Orthopyroxene is homogeneous, averaging $En_{58\pm2}$ (Table 4). Amphibole is edenite–hornblende (Table 5). Ilmenite and lesser amounts of titanomagnetite are present as single crystals, attached to rims, or as inclusions in

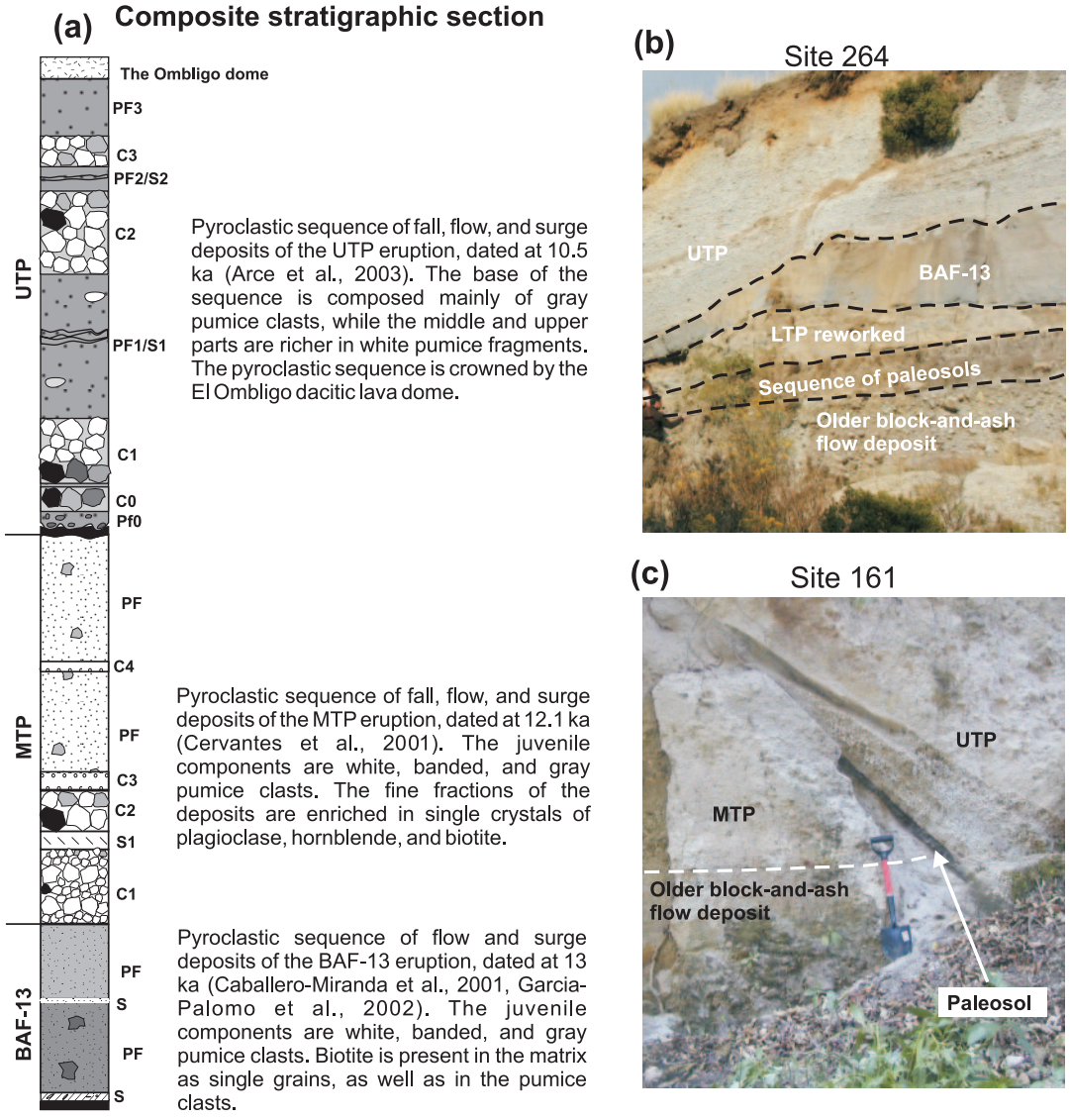

Fig. 2. (a) Composite stratigraphic column through the late Pleistocene–Holocene deposits of Nevado de Toluca volcano. BAF-13, block-and-ash flow of ~13 ka; MTP, Middle Toluca Pumice; UTP, Upper Toluca Pumice; S, pyroclastic surge; PF, pyroclastic flow; C, fall deposits. (b) Photograph of site 264 that shows the relationship between deposits UTP, BAF-13, LTP (Lower Toluca Pumice), and an older block-and-ash flow. The person is 1·8 m tall. (c) Photograph of site 161 showing the relationship between UTP, MTP, and an older block-and-ash flow deposit. The shovel is 50 cm long.

other phenocrysts (biotite, orthopyroxene and hornblende). Both ilmenite and titanomagnetite are the same composition in both white and grey pumice (Table 6).

Upper Toluca Pumice

Juvenile UTP samples consist of white pumice, grey pumice, and fragments of the Ombligo central dome, all of which are dacitic in composition, with very little variation amongst them (Fig. 3). All samples are porphyritic, with pumice containing 31–37 vol. % phenocrysts (vesicle free), and the dome fragments containing up to 43 vol. % (Table 1). Pumice is highly vesiculated with rhyolitic glass (Table 2) forming the bubble walls, whereas the dome rock has a microlite-rich matrix and only minor glass (Fig. 4, Table 1). In order of abundance, phenocrysts are plagioclase, orthopyroxene and hornblende, with minor Fe–Ti oxides, biotite and rare apatite (as inclusions in orthopyroxene). As in the BAF-13 and MTP samples, two populations of phenocrysts were observed; one including relatively small and euhedral phenocrysts (<1 mm diameter, Fig. 4), the other large phenocrysts (>1 mm to 2·3 mm diameter, Figs 4 and 5) with reaction rims, and resorbed margins. Biotite appears in different proportions in the UTP samples, often

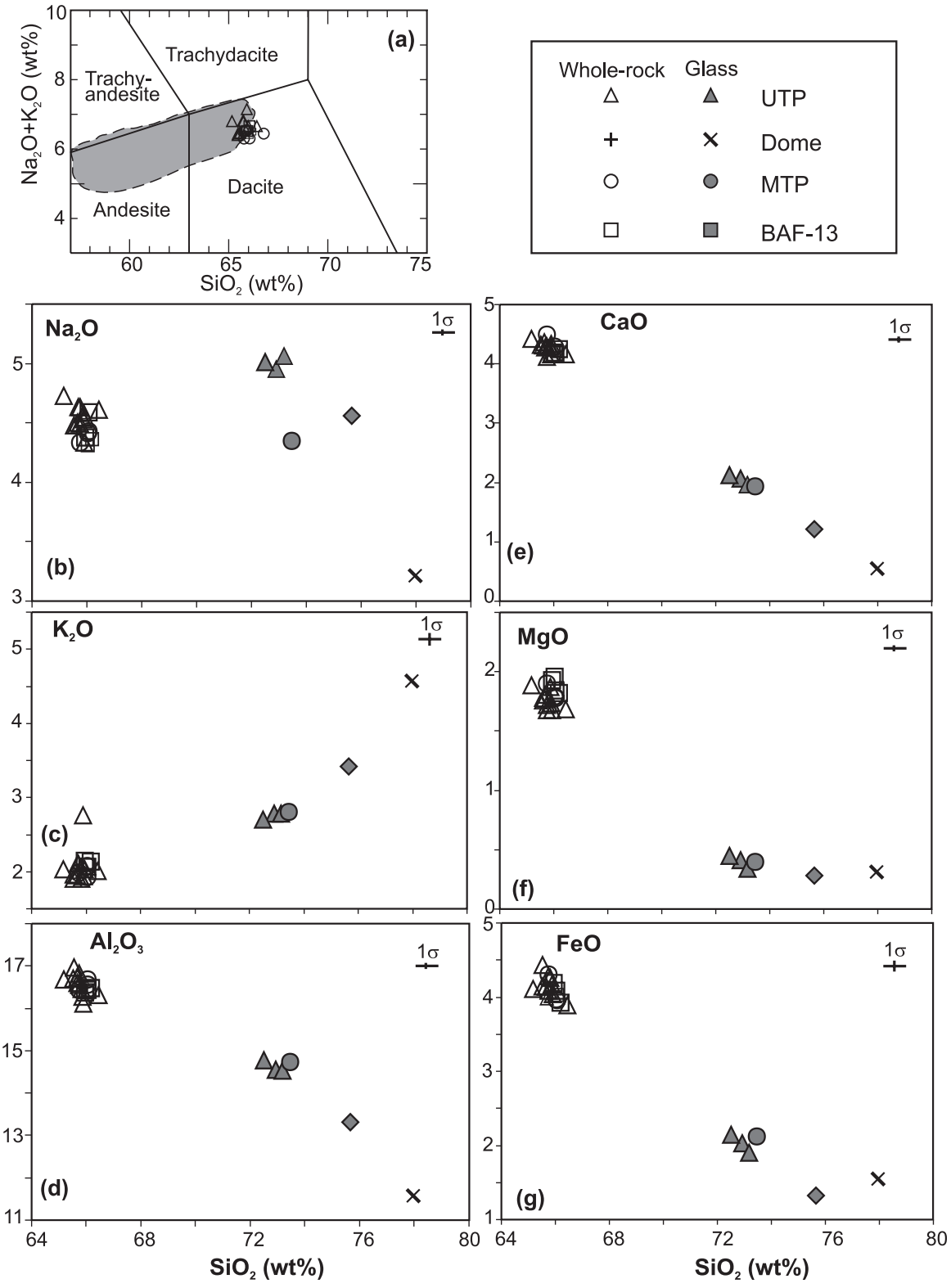

Fig. 3. (a) SiO_2 vs total alkalis diagram showing the composition of UTP, MTP, and BAF-13 rocks [modified from Le Bas *et al.* (1986)]. Grey field represents the range of compositions of Nevado de Toluca rocks. Data sources: Bloomfield & Valastro (1974); Macías *et al.* (1997); García-Palomo *et al.* (2002). (b–g) Binary diagrams of silica vs major elements for whole rocks and electron microprobe analyses of glasses. All samples were plotted on a water-free basis. Open symbols are whole-rock data; filled symbols are electron microprobe data for interstitial glasses.

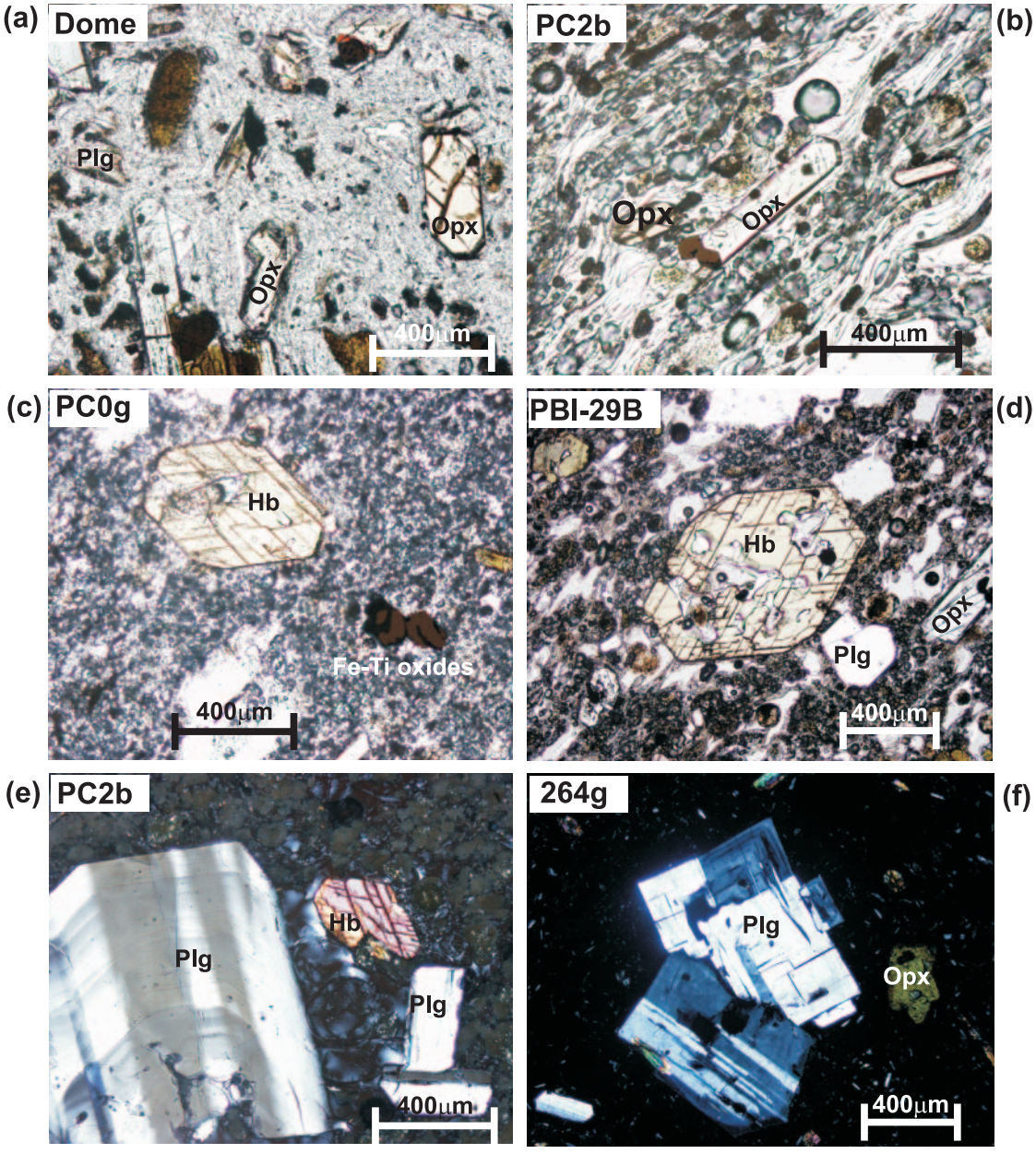

Fig. 4. (a–d) Plane-polarized light photomicrographs. (a) Ombligo dome, with phenocrysts of stable orthopyroxene (Opx) and plagioclase (Plg) in a microlitic matrix; (b) white pumice of the UTP deposit, showing some stable Opx phenocrysts set in a fibrous–glassy matrix; (c) grey pumice of the UTP deposit, with stable hornblende (Hb) and Fe–Ti oxides; (d) grey pumice of the MTP with stable Hb, Plg, and Opx phenocrysts. (e, f) Cross-polarized light photomicrographs. (e) White pumice of the UTP deposit showing stable Plg, and Hb phenocrysts; (f) grey pumice of the BAF-13 deposit with stable plagioclase and resorbed Opx phenocrysts in a glassy matrix.

<0·1 vol. %. It occurs only as large (>1 mm diameter) phenocrysts (never as microlites). Biotite appears either rimmed with small intergrowths of amphibole, orthopyroxene, Fe–Ti oxides, and plagioclase, or with resorbed margins (Fig. 5).

Plagioclase varies in abundance between UTP samples (Table 1). Euhedral, subhedral, and resorbed margins are observed in all samples. Plagioclase in the white pumice varies from An_{47} cores to $An_{47\pm2}$, whereas in the grey pumice it varies from An_{44} cores to $An_{40\pm8}$ rims (Table 3). Plagioclase in the dome samples varies from $An_{33\pm2}$ cores to $An_{40\pm10}$ rims. Small (<1 mm diameter) phenocrysts are $An_{40\pm7}$ (Table 3).

Orthopyroxene represents 4–5 vol. % of the UTP samples (Table 1) and is present either as large (>1 mm diameter) phenocrysts with corrosion enbayments and

Table 1: Modal mineralogy of pumice samples from the UTP, MTP, and BAF-13 deposits and the lava dome of Nevado de Toluca volcano

Unit	Site no.	Sample	Rock type	No. counts	Plg	Opx	Hb	Bt	Ox	Cum	Gmass
UTP	161	PC0g	grey pumice	1000	30·34	3·79	2·41	0·00	0·69	0·34	62·41
UTP	161	PC2b	white pumice	1000	24·60	5·50	0·85	0·14	0·63	0·00	68·29
Dome	9596	9596	lava	1000	35·21	5·39	1·20	0·24	0·12	0·96	56·89
MTP	161	PBI-2A	white pumice	1000	24·17	8·16	0·91	0·00	0·00	0·30	66·47
MTP	161	PBI-2B	grey pumice	863	36·50	9·05	1·81	0·15	0·90	0·00	51·58
BAF-13	264	264-wpf	white pumice	1000	37·50	10·46	4·62	0·04	0·92	0·00	46·46
BAF-13	264	264-gpf	grey pumice	525	36·70	6·52	1·64	0·12	1·52	0·00	53·50

Phenocrysts (>0·03 mm), vesicles, and groundmass (glass + microlites) were considered. Plg, plagioclase; Opx, orthopyroxene; Hb, hornblende; Bt, biotite; Ox, Fe–Ti oxides; Cum, clots of opx + hb + plg; Gmass, groundmass.

Table 2: Selected electron microprobe glass composition in the UTP and MTP samples

Unit:	UTP					MTP
Sample:	PC0g	PC1b	PC2A*	PC3	Dome	PBI-2A
	gp	wp	wp	wp	lava	wp
Matrix glass						
SiO_2	75·65 (1·37)	73·18 (0·11)	72·50 (0·33)	72·92 (0·30)	77·97 (3·22)	73·46 (0·70)
TiO_2	0·19 (0·11)	0·22 (0·01)	0·25 (0·07)	0·26 (0·08)	0·26 (0·19)	0·19 (0·11)
Al_2O_3	13·31 (1·10)	14·53 (0·15)	14·78 (0·06)	14·55 (0·13)	11·57 (0·99)	14·73 (0·41)
FeO†	1·32 (0·20)	1·90 (0·08)	2·14 (0·23)	2·03 (0·38)	1·54 (0·95)	2·12 (0·23)
MnO	0·05 (0·04)	0·02 (0·01)	0·04 (0·03)	0·04 (0·03)	0·04 (0·02)	n.d.
MgO	0·28 (0·13)	0·34 (0·02)	0·45 (0·03)	0·41 (0·05)	0·32 (0·30)	0·40 (0·03)
CaO	1·22 (0·47)	1·96 (0·02)	2·13 (0·06)	2·06 (0·14)	0·54 (0·37)	1·94 (0·30)
Na_2O	4·56 (0·36)	5·06 (0·03)	5·01 (0·26)	4·95 (0·24)	3·21 (0·67)	4·35 (0·53)
K_2O	3·42 (0·41)	2·78 (0·04)	2·70 (0·16)	2·78 (0·07)	4·56 (1·21)	2·81 (0·05)
Total	96·42	99·80	99·76	98·93	98·21	96·57
n	6	2	6	7	8	5

These data represent average values (in wt %) of the total number of analyses (*n*) and the standard deviation in parentheses. Analyses are normalized to 100%; however, the non-normalized total is reported. wp, white pumice; gp, grey pumice; n.d., not determined.
*This sample was used as the starting material in the hydrothermal experiments.
†Total Fe as FeO.

resorbed rims, or small (<1 mm diameter), euhedral phenocrysts (Fig. 4). No substantial compositional variations exist, however; in the white pumice orthopyroxene is $En_{56\pm1·5}$, in the grey pumice it is $En_{57\pm3·5}$, and in the dome, $En_{59\pm1·5}$ (Table 4). Amphibole phenocrysts are euhedral and range in size significantly. In addition, some of the larger phenocrysts have inner dissolution zones (Fig. 4). Compositions vary little between cores and rims (Table 5) and are generally edenite to pargasite–hornblende. Biotite represents <1 vol. % in the UTP samples, and was classified as ferroan–phlogopite (Table 5). Ilmenite and lesser titanomagnetite are present attached to phenocrysts (mainly of hornblende and orthopyroxene) or as individual crystals in the matrix. Ilmenite is Ilm 0·83–0·87 and titanomagnetite is Usp 0·27–0·48 (Table 6).

Summary of petrography

Juvenile fragments from the BAF-13, MTP, and UTP deposits have the same textures, mineral assemblage, and

Table 3: Compositions and structural formulae (8 O) of plagioclase in the UTP, MTP, and BAF-13 samples

Sample	SiO_2	Al_2O_3	FeO*	CaO	Na_2O	K_2O	Total	Si	Al	Fe	Ca	Na	K	Ab	An	Or	*n*
UTP samples																	
PC0g																	
core	56·21	27·39	0·20	8·94	6·13	0·31	99·18	10·18	5·84	0·03	1·73	2·15	0·07	54·40	43·80	1·80	1
rim	58·43 (2·96)	26·88 (1·58)	0·17 (0·06)	8·21 (1·69)	6·72 (0·54)	0·32 (0·08)	100·73	10·38	5·63	0·03	1·56	2·32	0·07	58·62	39·57	1·80	6
Mc	60·28	25·91	0·12	7·63	7·24	0·36	101·54	10·61	5·37	0·02	1·44	2·47	0·08	61·90	36·00	2·00	1
PC1b																	
rim	55·82 (1·05)	28·64 (0·57)	0·23 (0·13)	9·98 (0·75)	5·94 (0·55)	0·23 (0·03)	100·83	9·97	6·03	0·03	1·91	2·06	0·05	51·10	47·58	1·28	4
core	56·24 (1·20)	27·97 (0·10)	0·29 (0·05)	9·86 (0·24)	5·76 (0·19)	0·26 (0·09)	100·37	10·08	5·91	0·04	1·89	2·00	0·059	50·6	47·85	1·55	2
PC3																	
core	58·68	27·66	0·15	8·08	6·70	0·34	101·61	10·33	5·74	0·02	1·52	2·29	0·076	58·8	39·2	2·00	1
c-r	56·58 (0·27)	28·02 (0·15)	0·25 (0·06)	10·05 (0·09)	5·95 (0·01)	0·24 (0·01)	101·08	10·08	5·88	0·04	1·92	2·06	0·0545	51·05	47·6	1·35	2
rim	56·23 (1·45)	28·16 (0·95)	0·25 (0·09)	9·85 (0·77)	5·86 (0·55)	0·24 (0·05)	100·59	10·06	5·93	0·04	1·89	2·03	0·06	51·10	47·50	1·40	9
Mc	56·22 (2·02)	27·95 (0·77)	0·25 (0·02)	9·09 (0·94)	6·23 (0·47)	0·26 (0·04)	99·98	10·10	5·92	0·04	1·75	2·17	0·06	54·55	43·95	1·50	2
Dome																	
core	59·87 (0·62)	25·35 (0·31)	0·40 (0·04)	6·89 (0·39)	7·40 (0·17)	0·44 (0·07)	100·34	10·66	5·32	0·06	1·31	2·55	0·10	64·35	33·15	2·50	2
rim	58·35 (0·90)	26·65 (1·50)	0·31 (0·19)	7·96 (0·63)	6·79 (10·81)	0·32 (0·11)	100·35	10·35	5·66	0·05	1·58	2·30	0·07	58·21	40·04	1·75	8
Mc	58·25 (1·50)	26·81 (1·34)	0·16 (0·14)	8·23 (0·31)	6·56 (0·78)	0·31 (0·08)	100·32	10·39	5·63	0·02	1·57	2·27	0·07	57·90	40·28	1·83	4
MTP samples																	
PBI-29A																	
core	56·69 (1·29)	28·01 (0·15)	0·17 (0·07)	9·46 (1·28)	6·00 (0·47)	0·25 (0·08)	100·57	10·12	5·89	0·03	1·81	2·08	0·06	52·65	45·90	1·45	4
c-r	56·34 (1·27)	28·03 (0·70)	0·25 (0·04)	9·55 (0·87)	5·91 (0·45)	0·21 (0·04)	100·28	10·10	5·92	0·04	1·83	2·05	0·05	52·17	46·57	1·27	3
rim	56·40 (0·37)	28·07 (0·41)	0·26 (0·08)	9·57 (0·23)	5·92 (0·20)	0·24 (0·02)	100·46	10·08	5·92	0·04	1·85	2·04	0·06	51·70	46·83	1·48	4
Mc	56·91	27·77	0·21	9·28	5·93	0·23	100·33	10·08	5·92	0·04	1·85	2·04	0·06	51·70	46·83	1·48	1
PBI-29B																	
core	55·70 (1·17)	28·21 (0·95)	0·21 (0·19)	9·87 (0·77)	5·73 (0·49)	0·23 (0·05)	99·95	10·02	5·98	0·04	1·93	1·97	0·05	49·95	48·75	1·28	4
c-r	55·59	28·65	0·26	10·53	5·38	0·23	100·63	9·95	6·04	0·04	2·02	1·87	0·05	47·40	51·30	1·30	1
rim	56·55 (0·44)	27·83 (0·32)	0·27 (0·11)	9·33 (0·16)	6·09 (0·31)	0·24 (0·02)	100·31	10·11	5·90	0·04	1·79	2·11	0·06	53·40	45·20	1·40	4
Mc	56·670·95)	27·78 (0·23)	0·21 (0·07)	9·38 (0·35)	6·07(0·18)	0·25 (0·02)	100·36	10·16	5·83	0·04	1·79	2·13	0·06	53·47	45·00	1·50	3
BAF-13 samples																	
264																	
core	57·59 (1·95)	27·30 (1·41)	0·34 (0·07)	9·33 (1·49)	6·12 (0·51)	0·22 (0·04)	100·9	10·25	5·73	0·05	1·78	2·11	0·05	53·54	45·16	1·26	5
c-r	57·43 (0·68)	26·93 (0·53)	0·41 (0·01)	9·13 (0·10)	6·43 (0·04)	0·24 (0·00)	100·58	10·27	5·67	0·06	1·75	2·23	0·05	55·25	43·40	1·35	2
rim	57·07 (0·92)	27·66 (0·28)	0·46 (0·02)	9·81 (0·34)	5·90 (0·25)	0·22 (0·04)	101·12	10·21	5·74	0·07	1·82	2·08	0·05	52·70	46·02	1·26	5
Mc	58·35 (0·98)	27·50 (1·11)	0·50 (0·09)	9·42 (1·33)	6·20 (0·47)	0·22 (0·04)	102·2	10·26	5·696	0·073	1·776	2·112	0·05	53·64	45·1	1·27	7

Values are averages (in wt %) of *n* analyses and the standard deviation in parentheses. c, core; r, rim; c-r, midpoint between core and rim; Mc, microphenocryst.
*Total Fe as FeO.

mineral composition. All samples contain two populations of phenocrysts: large phenocrysts with resorption textures and small, euhedral phenocrysts (Figs 4 and 5). Biotite is present only as large phenocrysts and is always partially resorbed or rimmed by reaction products. The lack of euhedral microphenocrystic biotite suggests that it is not stable in the three magmas.

Crystallinity varies amongst the samples; the Ombligo dome contains 43 vol. % crystals, followed by the grey pumice (38–48 vol. %), and the white pumice (~34 vol. %) (Table 1). Glass composition also varies; the dome samples contain the most evolved glass (78 wt % SiO_2), followed by the grey pumice (76 wt % SiO_2), and the white pumice (72–73 wt % SiO_2) (Fig. 3). The whole-rock

Table 4: Compositions and structural formulae (6 O) of orthopyroxene from the UTP, MTP, and BAF-13 samples

Unit:	UTP					MTP		**BAF-13**
Sample:	PC0g	PC1b	PC2A	PC3	Dome	PBI-2A	PBI-29b	264
	gp	wp	wp	wp		wp	gp	wp
SiO_2	49·31 (0·36)	50·18 (1·36)	50·14 (1·33)	50·43 (1·66)	52·27 (0·56)	51·83 (0·11)	51·91 (0·18)	53·26 (0·05)
TiO_2	0·25 (0·05)	0·12 (0·10)	0·24 (0·10)	0·12 (0·11)	0·13 (0·12)	0·06 (0·05)	0·17 (0·14)	0·18 (0·01)
Al_2O_3	1·19 (0·18)	1·00 (0·16)	0·85 (0·25)	0·85 (0·28)	0·73 (0·29)	0·96 (0·25)	0·92 (0·36)	1·14 (0·02)
FeO*	27·09 (0·03)	26·07 (0·50)	26·86 (1·42)	26·25 (0·90)	24·17 (0·86)	24·27 (0·21)	24·28 (0·95)	24·56 (0·11)
MnO	0·65 (0·05)	0·59 (0·19)	0·56 (0·21)	0·65 (0·07)	0·65 (0·18)	0·59 (0·01)	0·67 (0·05)	0·64 (00·03)
MgO	20·35 (0·05)	20·89 (0·10)	20·67 (0·49)	20·98 (0·38)	20·65 (1·04)	20·09 (0·13)	20·02 (0·98)	21·09 (0·17)
CaO	0·91 (0·42)	0·84 (0·13)	0·74 (0·18)	0·89 (0·09)	0·74 (0·19)	0·74 (0·01)	0·78 (0·25)	0·88 (0·05)
Total	99·8	99·76	100·09	100·23	99·37	98·61	98·81	101·76
Si	1·87	1·90	1·89	1·89	1·98	1·98	1·98	1·97
Al	0·05	0·04	0·04	0·05	0·02	0·02	0·02	0·03
Ti	0·01	0·00	0·01	0·01	0·00	0·00	0·00	0·01
Fe^{3+}	0·08	0·06	0·07	0·05	0·00	0·00	0·00	0·00
Mg	0·88	0·90	0·90	0·89	0·98	0·97	0·97	0·97
Fe^{2+}	0·66	0·66	0·69	0·66	0·76	0·78	0·77	0·75
Mn	0·02	0·02	0·02	0·02	0·02	0·02	0·02	0·02
Ca	0·04	0·03	0·03	0·05	0·03	0·03	0·03	0·04
Na	0·00	0·00	0·00	0·01	0·00	0·00	0·00	0·00
K	0·00	0·00	0·00	0·00	0·00	0·00	0·00	0·00
WO	1·78	1·66	1·46	2·22	1·52	1·55	1·63	1·81
EN	55·65	57·30	56·49	56·96	58·81	58·10	57·88	58·98
FS	42·57	41·04	42·05	40·82	39·68	40·35	40·49	39·21
n	3	3	5	5	10	2	12	3

All values are averages (in wt %) of *n* analyses and the standard deviation in parentheses. gp, grey pumice; wp, white pumice.
*Total Fe as FeO.

compositions of the three deposits are very similar (63–65 wt % SiO_2), however, suggesting that the variations in the glass composition are a function of the crystal content.

GEOTHERMOMETRY

The presence of ilmenite and magnetite in all samples allows us to estimate pre-eruptive temperature (T) and oxygen fugacity (f_{O_2}), reported referenced to the fayalite–magnetite–quartz (FMQ) buffer. These parameters were calculated using the QUILF program of Andersen *et al.* (1993). Each titanomagnetite composition was combined with each ilmenite found in the same sample to obtain a range of T and f_{O_2}.

For the BAF-13 sample one titanomagnetite crystal and four ilmenite crystals were analyzed (Table 6) and give an equilibrium temperature of 812–829°C (819 ± 7°C average) and $\Delta\log f_{O_2}$ (FMQ) = 1·76–1·93 (1·84 ± 0·09 average) (Table 6; Fig. 6). For the MTP pumice, a total of three titanomagnetite and six ilmenite crystals in sample PBI2A and six ilmenite crystals in sample PBI29B were analyzed (Table 6). Assuming that the magnetites in PBI2A represent equilibrium compositions with ilmenite in the PBI29B pumice, we estimate the temperature and oxygen fugacity for the MTP as 796–809°C (802 ± 7°C average) and $\Delta\log f_{O_2}$ (FMQ) = 0·82–0·96 (0·89 ± 0·07 average). For the UTP deposit, we obtain equilibrium temperatures of 812–837°C (824 ± 12°C average) and $\Delta\log f_{O_2}$ (FMQ) = 1·31–1·40 (1·37 ± 0·07 average) (Table 6; Fig. 6) in white pumice and 829°C and $\Delta\log f_{O_2}$ (FMQ) = 1·30 for the grey pumice. A much higher (and a large range) temperature of 846–877°C (865 ± 19°C average) and $\Delta\log f_{O_2}$ (FMQ) = 0·70–0·90 (0·79 ± 0·09 average) was obtained for the dome (Fig. 6).

There are some temperature variations between samples; the MTP magma was ~20°C and the BAF-13 ~5°C cooler than the UTP, whereas the dome was ~40°C hotter than the UTP magma. The high temperature of

Table 5: Compositions and structural formulae of amphibole (23 O) and biotite (22 O) from the UTP, MTP, and BAF-13 samples

Unit:	UTP						MTP		BAF-13	
Sample:	PC0g	PC1b	PC2A	PC3	Dome	Dome	PBI-2A	PBI-29b	264	264
	gp	wp	wp	wp	Lava	Lava	wp	gp	wp	wp
Mineral:	Amph	Amph	Amph	Amph	Amph	Bt	Amph	Amph	Amph	Bt
SiO_2	43·96 (2·08)	43·46 (1·43)	43·36 (1·80)	43·21 (1·53)	45·19 (1·12)	37·52 (0·11)	44·45 (0·28)	44·581·13)	44·57 (1·28)	37·05 (0·37)
TiO_2	1·73 (1·02)	1·82 (1·04)	2·02 (1·42)	1·98 (0·47)	1·55 (0·64)	4·09 (0·20)	1·79 (0·58)	1·94 (0·65)	1·57 (0·39)	3·64 (0·12)
Al_2O_3	9·73 (0·85)	9·91 (1·60)	10·01 (2·77)	10·06 (0·84)	9·84 (1·50)	15·09 (0·18)	10·52 (0·37)	9·80 (0·67)	10·46 (0·94)	14·74 (1·11)
FeO*	16·90 (0·93)	16·30 (1·69)	15·23 (3·68)	16·41 (0·95)	15·54 (1·44)	16·40 (0·20)	14·51 (0·61)	15·47 (1·18)	16·95 (2·85)	18·10 (0·56)
MnO	0·23 (0·08)	0·18 (0·14)	0·27 (0·19)	0·29 (0·14)	0·31 (0·19)	0·13 (0·04)	0·19 (0·06)	0·27 (0·04)	0·31 (0·10)	0·13 (0·04)
MgO	12·92 (0·54)	12·77 (1·60)	13·31 (0·67)	13·17 (1·73)	12·54 (1·42)	14·12 (0·17)	12·76 (0·35)	12·65 (0·67)	12·28 (1·16)	13·39 (1·21)
CaO	10·66 (0·50)	10·77 (0·93)	11·24 (1·16)	10·63 (0·50)	10·29 (0·49)	0·07 (0·02)	10·78 (0·43)	10·32 (0·18)	10·50 (0·57)	0·10 (0·07)
Na_2O	1·89 (0·38)	1·94 (0·36)	2·03 (0·58)	2·01 (0·13)	1·83 (0·40)	0·89 (0·09)	1·87 (0·12)	1·80 (0·12)	1·99 (0·13)	0·44 (0·08)
K_2O	0·39 (0·06)	0·45 (0·12)	0·37 (0·16)	0·43 (0·05)	0·44 (0·09)	7·59 (0·26)	0·48 (0·05)	0·38 (0·03)	0·34 (0·01)	7·80 (1·25)
F	n.a.	n.a.	n.a.	n.a.	n.a.	n.a.	n.a.	n.a.	n.a.	0·20 (0·15)
Total	98·43	97·06	97·86	98·19	97·58	95·92	97·43	97·25	99·02	95·60
Si	6·44	6·48	6·45	6·44	6·70	5·81	6·58	6·64	6·65	5·82
Al	1·56	1·52	1·55	1·56	1·30	2·19	1·42	1·36	1·35	2·18
Fe	1·57	1·69	1·60	1·65	1·64	2·12	1·56	1·62	1·61	2·38
Mg	2·96	2·91	2·95	2·93	2·77	3·26	2·82	2·81	2·73	3·14
Mn	0·02	0·03	0·02	0·04	0·04	0·02	0·02	0·03	0·04	0·02
Ca	1·61	1·61	1·67	1·57	1·63	0·01	1·70	1·64	1·45	0·02
Na	0·58	0·56	0·59	0·58	0·48	0·27	0·51	0·50	0·58	0·13
K	0·08	0·08	0·07	0·08	0·08	1·50	0·09	0·07	0·06	1·56
Ti	0·22	0·22	0·23	0·22	0·17	0·48	0·20	0·22	0·18	0·43
n	6	9	7	10	12	3	4	3	3	5

All values are averages (in wt %) of *n* analyses and the standard deviation in parentheses. gp, grey pumice; wp, white pumice; n.a., not analyzed; Amph, amphibole; Bt, biotite.
*Total Fe as FeO.

the dome (865°C average) is a puzzle, considering that slow cooling systems typically experience re-equilibration of the oxides with time (Hammond & Taylor, 1982). This temperature for the dome reflects the different composition of the titanomagnetite (Table 6). To constrain the extent of Fe–Ti oxide re-equilibration, we calculated maximum oxygen fugacities and temperatures for the three magmas utilizing the compositions of orthopyroxene, magnetite, and ilmenite in our samples, and assuming that the silica activity was nearly unity. Interestingly, the temperatures and oxygen fugacities obtained are very similar to those calculated with the two oxides, even for the dome (see Fig. 6), which again yields a higher temperature (869 ± 15°C). This indicates that orthopyroxene, titanomagnetite, and ilmenite are in equilibrium in all rocks, except for the dome, which displays a large temperature range (Fig. 6). The presence of large phenocrysts and microlites in the dome samples suggest that the magma underwent slow ascent and cooling, promoting rapid re-equilibration of the Fe–Ti oxides as proposed elsewhere (e.g. Frost, 1991; Lindsley *et al.*, 1991; Venezky & Rutherford, 1999). This process modified the Fe–Ti oxide compositions resulting in an apparently higher temperature. The three magmas have a temperature range from 795 to 885°C (Fig. 6). $\Delta\log f_{O_2}$ is highest in the MTP.

$^{40}Ar/^{39}Ar$ DATING AND BIOTITE SOURCE

Microphenocrysts of plagioclase, orthopyroxene, hornblende, and Fe–Ti oxides are euhedral and appear to be in equilibrium with the surrounding matrix. In contrast the larger phenocrysts (up to 2·3 mm diameter), including biotite, appear to be partially resorbed. Biotite has reaction rims of hornblende, orthopyroxene, and plagioclase (Fig. 5), suggesting that it may be xenocrystic.

Table 6: Compositions of Fe–Ti oxides in the UTP, MTP, and BAF-13 samples

		Al_2O_3	MgO	TiO_2	Cr_2O_3	FeO*	MnO	NiO	Total	f_{O_2}	T(°C)	ΔFMQ	X_{Ilm}	X_{Usp}	Ti	Al	Fe^{2+}	Fe^{3+}	Mg	Mn
UTP samples																				
PC3	Ilm1	0·24	2·29	43·89	0·03	49·64	0·45	0·09	96·63	−12·29	837	1·36	0·83		0·84	0·01	0·74	0·31	0·09	0·01
PC3	Ilm2	0·27	2·31	44·14	0·11	49·04	0·33	0·16	96·36	−12·56	824	1·34	0·84		0·85	0·01	0·75	0·30	0·09	0·01
PC3	Ilm3	0·21	2·23	44·32	0·08	49·01	0·22	0·14	96·21	−12·75	812	1·40	0·84		0·85	0·01	0·76	0·29	0·09	0·00
PC1b	Ilm4	0·23	2·26	44·33	0·09	49·89	0·30	0·00	97·11	−12·45	827	1·40	0·83		0·84	0·01	0·75	0·30	0·09	0·01
PC1b	Ilm5	0·24	2·35	45·03	0·11	49·46	0·31	0·00	97·50	−12·72	818	1·31	0·84		0·85	0·01	0·76	0·28	0·09	0·01
PC2A	Ilm6	0·27	2·34	44·57	0·13	50·01	0·30	0·04	97·66	−12·45	826	1·39	0·83		0·84	0·01	0·75	0·30	0·09	0·01
PC0 g	Ilm7	0·24	2·05	44·86	0·13	50·19	0·44	0·05	97·96	−12·51	829	1·30	0·84		0·85	0·01	0·76	0·29	0·08	0·01
PC1b	Tm1	2·70	1·29	10·17	0·76	79·82	0·21	0·09	95·04					0·30	0·29	0·12	1·21	1·30	0·07	0·01
Dome	Ilm8	0·24	1·06	44·68	0·05	50·03	0·32	0·02	96·47	−11·99	876	0·90	0·86		0·87	0·01	0·82	0·26	0·04	0·01
Dome	Ilm9	0·25	1·08	44·80	0·06	49·72	0·35	0·00	96·31	−12·08	874	0·83	0·87		0·87	0·01	0·82	0·25	0·04	0·01
Dome	Ilm10	0·20	1·44	45·52	0·06	49·04	0·37	0·00	96·66	−12·44	859	0·76	0·87		0·09	0·01	0·82	0·24	0·06	0·01
Dome	Ilm11	0·25	1·05	44·43	0·10	49·64	0·34	0·00	95·89	−11·99	877	0·87	0·86		0·09	0·01	0·82	0·26	0·04	0·01
Dome	Ilm12	0·22	1·27	45·34	0·10	48·93	0·38	0·00	96·26	−12·47	860	0·72	0·88		0·88	0·01	0·82	0·23	0·05	0·01
Dome	Ilm13	0·27	1·27	45·15	0·07	49·63	0·39	0·05	96·87	−12·13	873	0·80	0·87		0·09	0·01	0·81	0·25	0·05	0·01
Dome	Ilm14	0·24	1·18	45·72	0·06	49·59	0·41	0·07	97·29	−12·39	865	0·70	0·88		0·88	0·01	0·83	0·24	0·05	0·01
Dome	Ilm15	0·20	1·11	45·78	0·06	49·78	0·32	0·00	97·29	−12·48	856	0·78	0·88		0·88	0·01	0·83	0·23	0·04	0·01
Dome	Ilm16	0·25	1·10	45·58	0·08	49·14	0·29	0·00	96·46	−12·70	846	0·77	0·88		0·88	0·01	0·84	0·22	0·04	0·01
Dome	Tm2	3·07	0·70	14·39	0·22	74·28	0·33	0·07	93·16					0·44	0·42	0·14	1·37	1·03	0·04	0·01
Dome	Tm3	2·92	0·61	15·34	0·11	72·96	0·34	0·00	92·32					0·48	0·45	0·13	1·40	0·97	0·04	0·01
Dome	Tm4	2·93	0·48	14·32	0·17	73·02	0·18	0·00	91·28					0·45	0·42	0·14	1·39	1·02	0·03	0·01
MTP samples																				
PBI-2A	Ilm2	0·21	2·32	45·94	0·06	47·47	0·36	0·01	96·38	−13·40	806	0·88	0·87		0·88	0·01	0·79	0·23	0·09	0·01
PBI-2A	Ilm3	0·22	2·24	45·52	0·07	46·98	0·31	0·00	95·40	−13·50	801	0·88	0·88		0·88	0·01	0·79	0·22	0·09	0·01
PBI-2A	Ilm4	0·39	2·39	44·88	0·13	46·67	0·29	0·00	95·76	−13·29	808	0·96	0·87		0·88	0·00	0·78	0·24	0·09	0·01
PBI-2A	Ilm5	0·22	2·31	46·44	0·06	47·53	0·36	0·00	96·93	−13·60	799	0·82	0·88		0·89	0·01	0·79	0·22	0·09	0·01
PBI-2A	Ilm6	0·23	2·29	46·06	0·10	47·47	0·36	0·00	96·50	−13·47	803	0·86	0·88		0·88	0·01	0·79	0·22	0·09	0·01
PBI-2A	Ilm7	0·25	2·34	46·18	0·06	47·55	0·36	0·00	96·77	−13·46	804	0·86	0·88		0·88	0·01	0·79	0·22	0·09	0·01
PBI-2B	Ilm8	0·23	2·35	46·11	0·09	47·32	0·27	0·00	96·41	−13·60	796	0·89	0·88		0·89	0·01	0·79	0·22	0·09	0·01
PBI-2B	Ilm9	0·22	2·31	46·18	0·08	47·72	0·30	0·02	96·89	−13·46	802	0·90	0·88		0·88	0·01	0·79	0·23	0·09	0·01
PBI-2B	Ilm10	0·25	2·44	45·87	0·11	47·69	0·32	0·00	96·74	−13·26	809	0·95	0·87		0·88	0·01	0·78	0·24	0·09	0·01
PBI-2B	Ilm11	0·21	2·01	46·06	0·09	48·24	0·34	0·00	96·98	−13·34	807	0·91	0·88		0·88	0·01	0·80	0·23	0·08	0·01
PBI-2B	Ilm12	0·22	2·27	46·18	0·11	47·22	0·33	0·03	96·36	−13·66	797	0·82	0·88		0·89	0·01	0·80	0·22	0·09	0·01
PBI-2B	Ilm14	0·21	2·28	46·01	0·11	47·28	0·27	0·11	96·26	−13·61	796	0·89	0·88		0·89	0·01	0·79	0·22	0·09	0·01
PBI-2A	Tmag1	2·55	1·30	11·03	0·48	75·51	0·26	0·00	91·23					0·34	0·32	0·12	1·24	1·23	0·08	0·01
PBI-2A	Tmag2	2·58	1·26	11·00	0·51	76·65	0·31	0·06	92·46					0·34	0·32	0·12	1·24	1·24	0·07	0·01
PBI-2A	Tmag3	2·57	1·28	10·84	0·49	76·29	0·19	0·01	91·76					0·34	0·32	0·12	1·24	1·25	0·07	0·01
BAF-13 samples																				
264	Ilm1	0·18	1·91	44·95	0·08	53·79	0·62	n.a.	101·54	−12·34	814	1·77	0·81		0·82	0·01	0·74	0·35	0·07	0·00
264	Ilm2	0·19	1·97	43·80	0·11	55·89	0·53	n.a.	102·49	−11·87	829	1·93	0·78		0·79	0·01	0·71	0·41	0·07	0·00
264	Ilm3	0·23	1·94	44·78	0·09	55·57	0·54	n.a.	103·14	−12·08	822	1·88	0·79		0·80	0·01	0·72	0·39	0·07	0·00
264	Ilm4	0·20	1·86	45·17	0·07	53·84	0·61	n.a.	101·74	−12·39	812	1·76	0·81		0·82	0·01	0·74	0·35	0·07	0·00
264	Tmag1	2·36	0·96	8·83	0·03	89·68	0·36	n.a.	102·23					0·24	0·23	0·10	1·17	1·44	0·05	0·01

Temperature (T) in degrees centigrades and oxygen fugacity (f_{O_2}) reported referenced to the fayalite–magnetite–quartz (FMQ) buffer calculated using the QUILF model (Andersen *et al.*, 1993). Ilm, Ilmenite; Tmt, Titanomagnetite; n.a., not analyzed. Values are given in wt %. Mole fractions and cation proportions of ilmenite (X_{Ilm}) and ulvöspinel (X_{Usp}) were also calculated by QUILF.
*Total Fe as FeO.

Table 7: Whole-rock compositions of the UTP, MTP, and BAF-13 rock samples

Unit:	UTP										
	[2]9596 dome	[2]185-AP wp	[2]185-BP wp	[2]185-CP wp	[2]185-DP wp	[2]9575 wp	3185-g gp	3285-g gp	[2]9570-fbp gp	[2]58Liti jl	[2]9570-fbl jl
Whole rock (wt %)											
SiO_2	64·28	63·27	63·41	63·59	64·19	64·08	63·32	63·92	64·26	65·70	65·46
TiO_2	0·60	0·63	0·62	0·61	0·60	0·62	0·65	0·62	0·61	0·63	0·63
Al_2O_3	16·08	16·37	16·15	15·99	16·43	16·34	16·21	16·15	16·21	16·07	16·49
Fe_2O_3*	4·16	4·00	4·00	3·90	3·99	4·34	3·99	3·87	3·95	4·11	4·26
MnO	0·08	0·06	0·06	0·06	0·06	0·08	0·06	0·06	0·08	0·07	0·07
MgO	1·73	1·70	1·71	1·67	1·68	1·70	1·83	1·76	1·63	1·73	1·67
CaO	4·21	4·13	4·21	4·18	4·19	4·22	4·30	4·16	4·12	4·15	4·10
Na_2O	4·46	4·31	4·35	4·43	4·39	4·38	4·59	4·51	4·43	4·32	4·61
K_2O	1·86	1·89	1·88	1·87	1·95	1·86	1·97	2·06	1·98	2·75	2·11
P_2O_5	0·20	0·18	0·18	0·18	0·17	0·16	0·24	0·20	0·17	0·17	0·18
LOI	0·96	2·78	2·90	2·73	2·60	2·35	1·73	1·55	1·62	1·73	1·24
Total	98·60	99·33	99·48	99·22	100·26	100·13	98·89	98·84	99·05	100·59	100·81

Unit:	UTP		MTP				BAF-13			
	[2]185-AJ jl	[2]185-BJ jl	[3]29Aw wp	[3]29Cg gp	[3]9545 wp	[1]9511 wp	[3]264g-f gp	[3]264g-s gp	[3]264w-f wp	[3]264w-s wp
Whole rock (wt %)										
SiO_2	64·41	64·67	64·93	65·06	63·99	65·67	65·35	64·59	65·06	64·78
TiO_2	0·63	0·59	0·64	0·64	0·58	0·59	0·62	0·61	0·61	0·63
Al_2O_3	15·92	15·88	16·40	16·32	15·99	15·95	16·21	16·04	16·19	16·12
Fe_2O_3*	4·08	3·79	3·90	3·90	4·19	3·78	3·99	4·10	3·86	4·01
MnO	0·06	0·06	0·06	0·06	0·07	0·06	0·07	0·07	0·07	0·07
MgO	1·83	1·64	1·76	1·75	1·85	1·51	1·82	1·89	1·79	1·92
CaO	4·19	4·05	4·22	4·17	4·37	3·90	4·12	4·09	4·17	4·11
Na_2O	4·43	4·49	4·34	4·36	4·22	4·21	4·54	4·29	4·29	4·23
K_2O	2·05	1·96	1·89	2·05	1·93	2·12	2·05	2·10	2·10	2·05
P_2O_5	0·18	0·21	0·19	0·19	0·14	0·13	0·17	0·17	0·17	0·17
LOI	2·00	1·48	1·77	1·38	2·27	2·60	1·22	1·88	1·55	2·19
Total	99·77	98·82	100·09	99·88	99·60	100·53	100·15	99·82	99·87	100·28

Analytical uncertainties are at the detection limit (0·01 wt %). Data from: [1]Macías *et al*. (1997); [2]Arce *et al*. (2003); [3]this study. wp, white pumice; gp, grey pumice; jl, juvenile lithic; LOI, loss on ignition. All data normalized to 100%, with original total listed.
*Total Fe given as Fe_2O_3.

The presence of hornblende in the rims suggests that the reaction occurred at high water pressures, and thus did not occur as a result of decompression during magma ascent (Rutherford & Hill, 1993). Instead, it probably occurred while the magma was stored in a deep reservoir.

To explore the possibility that the biotite is xenocrystic, we determined its Ar isotopic composition, because this technique has been used successfully to identify xenocrysts in other magmatic systems (e.g. Lo Bello *et al.*, 1987; Nelson *et al.*, 1992; Chen *et al.*, 1996; Singer *et al.*, 1998; Spell *et al.*, 2001; Gardner *et al.*, 2002).

Of the 30 biotite grains that were step-heated for $^{40}Ar/^{39}Ar$ dating (methods are described in Appendix A), only four grains showed fractions in the step-heating runs

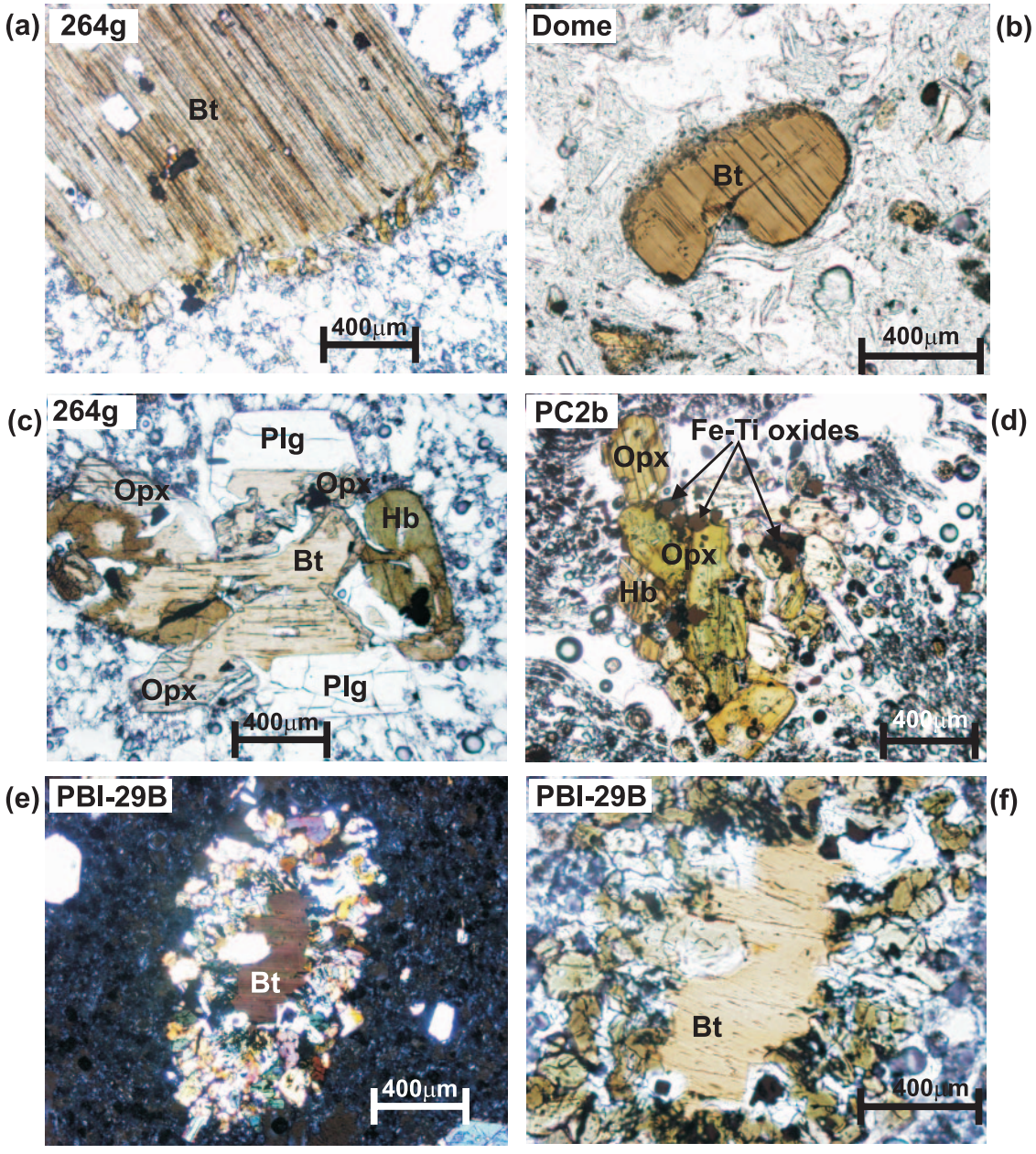

Fig. 5. Photomicrographs of biotite xenocrysts (Bt) found in the UTP, MTP, and BAF-13 samples. (a–d) Plane-polarized light photomicrographs: (a) a biotite xenocryst (2·3 mm) surrounded by a reaction rim composed of newly formed crystals of Opx, and Hb; (b) rounded biotite xenocryst with a thin reaction rim in the dome sample; (c) remnant biotite xenocryst surrounded by newly formed crystals of Opx, Hb, and Plg; (d) biotite has been completely replaced by new minerals. (e, f) Cross-polarized and plane-polarized light photomicrographs of remnant biotite xenocrysts (center) surrounded by new crystals.

with apparent ages, ranging from 4·7 to 0·8 Ma, that are significantly older than the late Pleistocene (13–10·5 ka) age of the deposits. The detailed analyses of these four grains are reported in Appendix B and the age spectra are shown in Fig. 7. The age spectra for the remaining 26 analyses have integrated ages that are indistinguishable from the eruption age, and/or do not show any fractions that are significantly older than the eruption age. The weighted mean apparent age of these grains is -23 ± 109 ka. This age is essentially zero (within 1σ error), but reflects that for some analyses, the apparent atmospheric argon percentage exceeded 100%, but not significantly. The poor precision of the analyses provides no additional information about the age of eruption or the potential presence of xenocrysts; consequently, the data are not included in the paper.

Table 8: Experimental conditions carried out on dacite white pumice (PC2A = sample 9575 in Table 7) of UTP deposit

Experiment	Starting material	Temperature (°C)	Pressure (MPa)	Duration (h)	Products
G-244B	PC2A	850	200	118	Glass + Plg + Amph + Opx + Ox
G-241	PC2A	780	200	186	Glass + Plg + Amph + Opx + Ox
G-247B	PC2A	880	200	69	Glass + Opx + Ox
G-256	PC2A	825	200	188	Glass + Plg + Amph + Opx + Ox
G-257B	PC2A	850	125	164	Glass + Plg + Opx + Ox
G-258B	PC2A	825	125	141	Glass + Plg + Opx + Ox
G-272A	G-247	840	150	327	Glass + Plg + Amph + Opx + Ox
G-272B	G-241	840	150	327	Glass + Plg + Amph + Opx + Ox
G-273	G-244B	820	150	327	Plg + Opx + Ox + Amph
G-287	PC2A	875	100	97	Glass + Opx + Ox
G-293	G-287	880	150	138	Opx + Ox
G-294	G-287	850	175	138	Plg + Opx + Amph + Ox
G-295B	G-287	800	250	164	Glass + Plg + Amph + Opx + Ox
G-296B	G-287	850	250	138	Glass + Amph + Opx + Ox
G-302A	G-256	875	100	210	Glass + Plg + Opx + Ox
G-302B	G-287	875	100	210	Glass + Plg + Amph + Opx + Ox
G-333	G-247B	800	150	476	Glass + Plg + Amph + Opx + Ox
G-334A	G-247B	850	250	363	Glass + Amph + Opx + Ox
G-336A	G-247B	880	150	219	Glass + Opx + Ox
G-336B	G-258B	880	150	219	Glass + Opx + Ox
G-362A	G-333	830	165	216	Opx + Plg + Ox + Amph
G-362B	G-287	830	175	216	Opx + Plg + Ox + Amph
G-363A	G-295B	860	200	216	Opx + Ox + Amph
G-363B	G-287	860	200	216	Opx + Ox + Amph

Starting material was either crushed UTP pumice (sample PC2A) or aliquots from previously run experiments.

Additionally, we used the composition of orthopyroxene and biotite determined by electron microprobe, with the model of Fonarev & Konilov (1986) to test if these mineral phases are in equilibrium in our samples. The results show that at temperatures of 800–840°C the iron content of the biotite is too high ($X_{bi}^{Fe} = 0{\cdot}61$—$0{\cdot}64$) to be in equilibrium with orthopyroxene ($X_{opx}^{Fe} = 0{\cdot}61$—$0{\cdot}64$); this further supports the idea that biotite is xenocrystic.

There are no known biotite-bearing rocks cropping out in the Toluca area that are ~4·7 Ma old or younger; thus we have no direct evidence that the biotite crystals are xenocrysts incorporated from the earlier products of the Nevado de Toluca volcano (which began erupting around 2·6 Ma; García-Palomo *et al.*, 2002). The only known biotite-bearing rocks below the volcano are within the 'Ixtapan–Teloloapan' metamorphic sequence of Late Jurassic–Cretaceous age, which consists of a wide variety of lithologies (volcanic rocks, sandstones, schists, phyllites, tuffs) (Campa *et al.*, 1974) and an ~55 Ma felsic intrusion

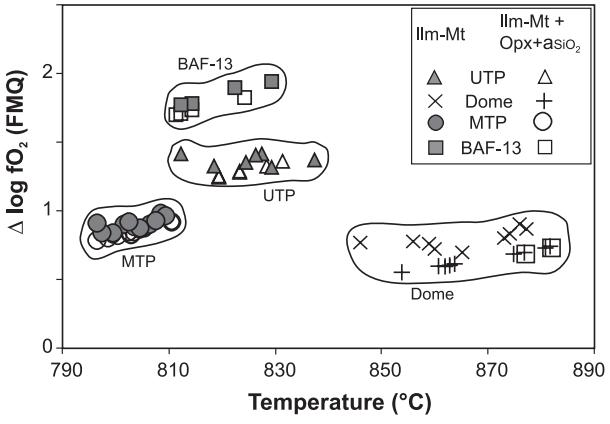

Fig. 6. Temperature–Δlog oxygen fugacity (FMQ) relationships for the UTP, MTP, and BAF-13 samples, calculated using the QUILF program (Andersen *et al.*, 1993). Grey symbols and × are temperatures calculated using coexisting Fe–Ti oxides; open symbols and + are temperatures calculated using Fe–Ti oxides plus orthopyroxene and assuming a silica activity of unity.

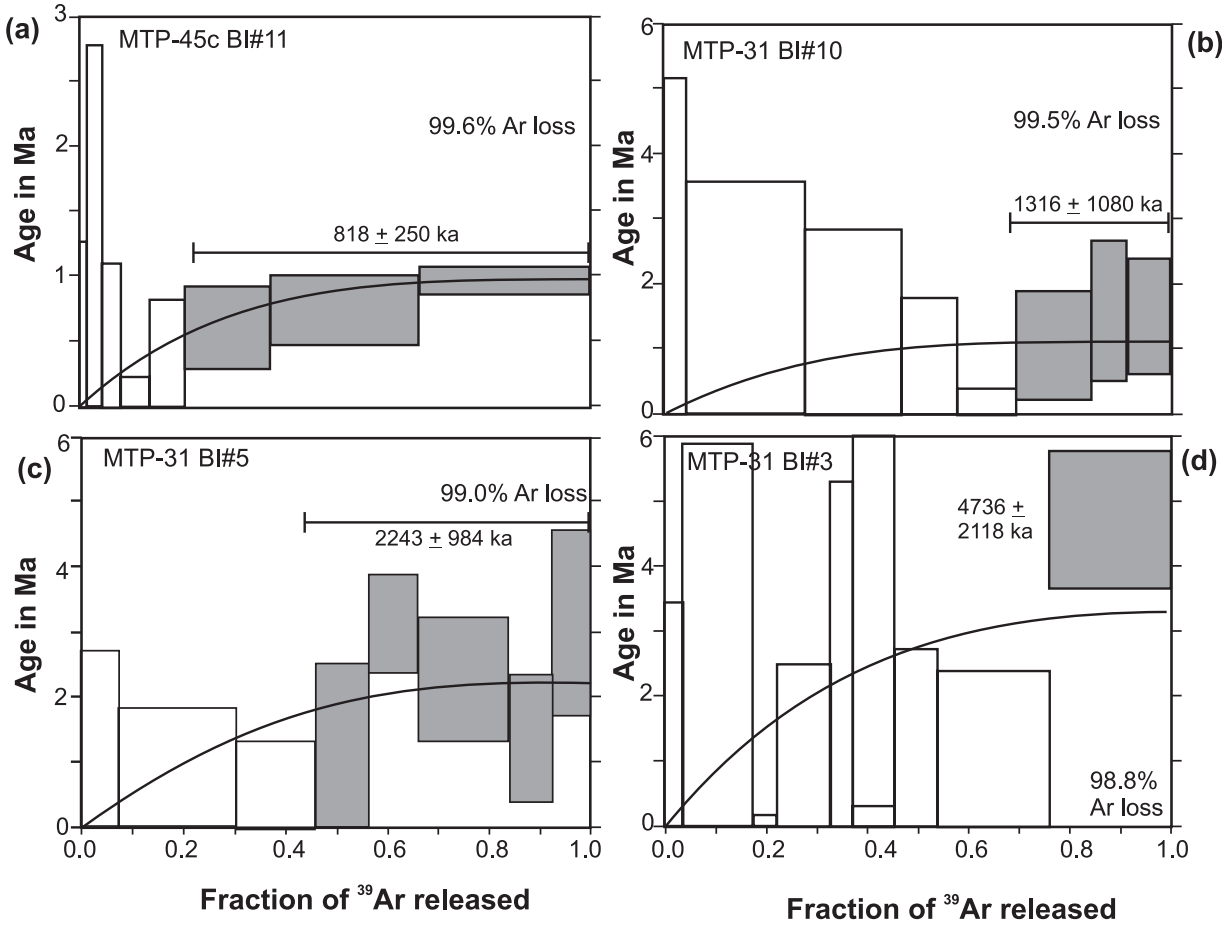

Fig. 7. $^{40}Ar/^{39}Ar$ age spectra ($\pm1\sigma$) for four biotite grains from the MTP deposit that show significant amounts of radiogenic ^{40}Ar. Grey boxes denote non-zero age fractions. Weighted mean ages (and $\pm2\sigma$ error) for these fractions are also shown. Diffusion loss profiles for each sample are denoted by the bold line. Profiles calculated assuming cylindrical diffusion, an original age of 150 Ma, a loss age of 0 Ma and Ar loss amounts ranging from 98·8% to 99·6% as noted for each sample (a–d). Diffusion profiles assuming an original age of 55 Ma, loss age of 0 Ma and Ar loss amounts ranging from 96·5% to 98·8% produce similar profiles.

(De Cserna *et al.*, 1974). If these rocks are potential sources of biotite xenocrysts, the age spectra could be consistent with incorporation of old biotite (>55 Ma) that would have lost significant amounts of argon (98–99%) by volume diffusion after incorporation in the magma (Fig. 7). Thus, our modeling implies an amount of argon loss that prevents us from determining the true source or age of the xenocrysts based on the age spectra alone.

As biotite xenocrysts would probably be highly reactive in the host dacitic magma they are likely to have only short residence time. The presence of reaction rims on the biotite crystals may have acted to reduce their contact with the melt, and hence extend their lifetimes. It is likely, however, that because biotite is present in all three of the eruptions, and those eruptions span about 2500 years, contamination by xenocryst incorporation was continual, and the biotite crystals in each of the deposits were introduced just prior to each eruption. At 800–850°C, which is the calculated range of temperature for the Toluca magmas (Fig. 6), 1 mm biotite crystals would be totally reset in about 1 year, based on the modeling approach of Gardner *et al.* (2002). It is, however, possible that some of the larger biotite xenocrysts would retain a trace of their original radiogenic argon, such as seen in the four crystals analyzed (Fig. 7). Relatively short times between incorporation and eruption have also been proposed for xenocrysts in other magmatic systems (e.g. Lo Bello *et al.*, 1987; Gardner *et al.*, 2002), although longer residence times have been proposed for plagioclase xenocrysts (Singer *et al.*, 1998).

It is noteworthy that the pumice clasts in the three deposits have a population of large phenocrysts of plagioclase, pyroxene, and hornblende with disequilibrium textures. These mineral phases may also represent xenocrysts incorporated into the magma, but because the latter was saturated with these phases, they did not completely dissolve.

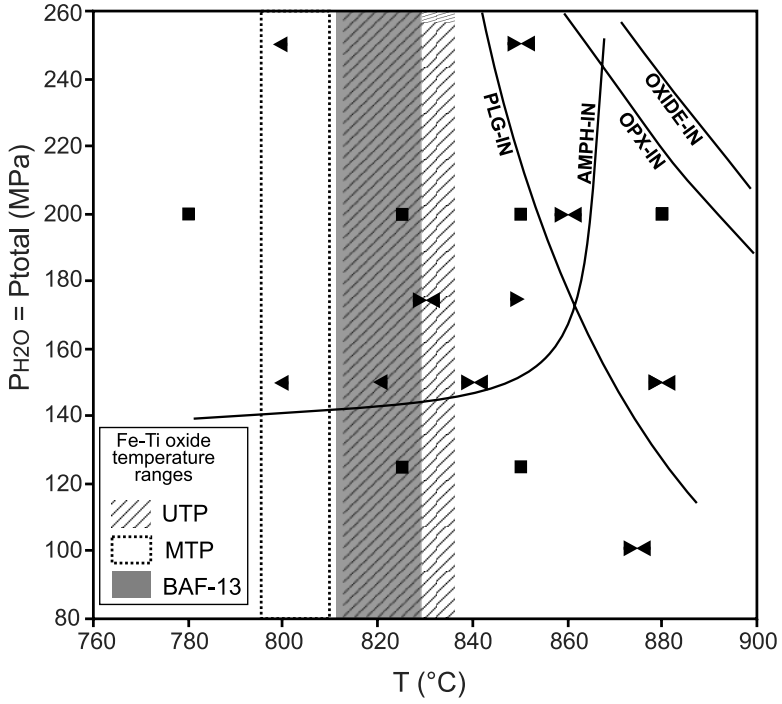

Fig. 8. Phase equilibria diagram obtained from hydrothermal experiments on the UTP dacite (sample PC2A), under H_2O-saturated conditions ($P_{H_2O} = P_{TOTAL}$). ■, runs that used natural powder. The arrowheads represent melting (pointing to the right) and crystallization (pointing to the left) experiments. All run conditions are listed in Table 8. Mineral-in curves are shown for orthopyroxene (Opx), amphibole (Amph), and plagioclase (Plg). The range of Fe–Ti oxide equilibration temperatures is shown for UTP, MTP, and BAF-13.

EXPERIMENTAL RESULTS

The three magmatic units studied (BAF-13, MTP, and UTP) are dacitic and consist of plagioclase, orthopyroxene, hornblende, and Fe–Ti oxides in a rhyolitic groundmass. To constrain the stability field of this mineral assemblage, we performed hydrothermal experiments using natural samples of UTP (see Appendix A for methods). All experiments were run water-saturated and above the solidus (all experimental conditions are listed in Table 8), and so all runs contain melt and water vapor. Orthopyroxene and Fe–Ti oxides were present in all the charges. The stabilities of plagioclase and hornblende vary with temperature and pressure (Fig. 8). Plagioclase stability decreases in temperature as water pressure increases, such that it is stable below 880°C at pressures below 140 MPa, but only below 850°C at 250 MPa. In contrast, hornblende is stable at higher temperatures as pressure increases. Hornblende is not stable below ~140 MPa or above 870°C. We note that the anomalously high temperatures of the dome sample obtained by Fe–Ti oxide geothermometry (846–877°C) are close to the upper stability limit of amphibole (Fig. 8). Above 860°C amphibole is unstable and does not coexist with plagioclase. In contrast, abundant hornblende and plagioclase exist together in the dome sample. Thus, those higher temperatures are not considered further. Despite the common presence of biotite in the natural samples, biotite did not crystallize in any of our experimental runs, and considering our petrographic observations that biotite is always resorbed or in reaction with the melt, the experimental results support the conclusion that biotite is xenocrystic. The experiments were run at $f_{O_2} \sim$ FMQ + 1·5 (NNO + 0·5, where NNO is the nickel–nickel oxide buffer). It could be argued that biotite might be stable under more oxidized conditions (e.g. Carmichael, 1991). We note, however, that even in our most oxidized sample (BAF-13) biotite is in reaction with the melt, and thus if biotite was originally phenocrystic it would require all of the magmas to have been much more oxidized (up to one log unit greater). This would not, however, explain the presence of older $^{40}Ar/^{39}Ar$ ages in biotite. In addition, it would require that each magma became reduced just before erupting, because no biotite could survive ~2500 years in a magma in which it is not stable. It has also been suggested that sulfur may help stabilize biotite (Costa & Pichavant, 2003; Costa *et al.*, 2004). Electron microprobe analyses of biotite crystals in the Toluca samples did not detect sulfur, suggesting that its presence was not important in these magmas. We believe, therefore, that our experimental results are consistent with the conclusion that biotite is xenocrystic in the three magmas.

Residual melt (quenched to glass) is the most abundant phase in all the experimental runs and varies

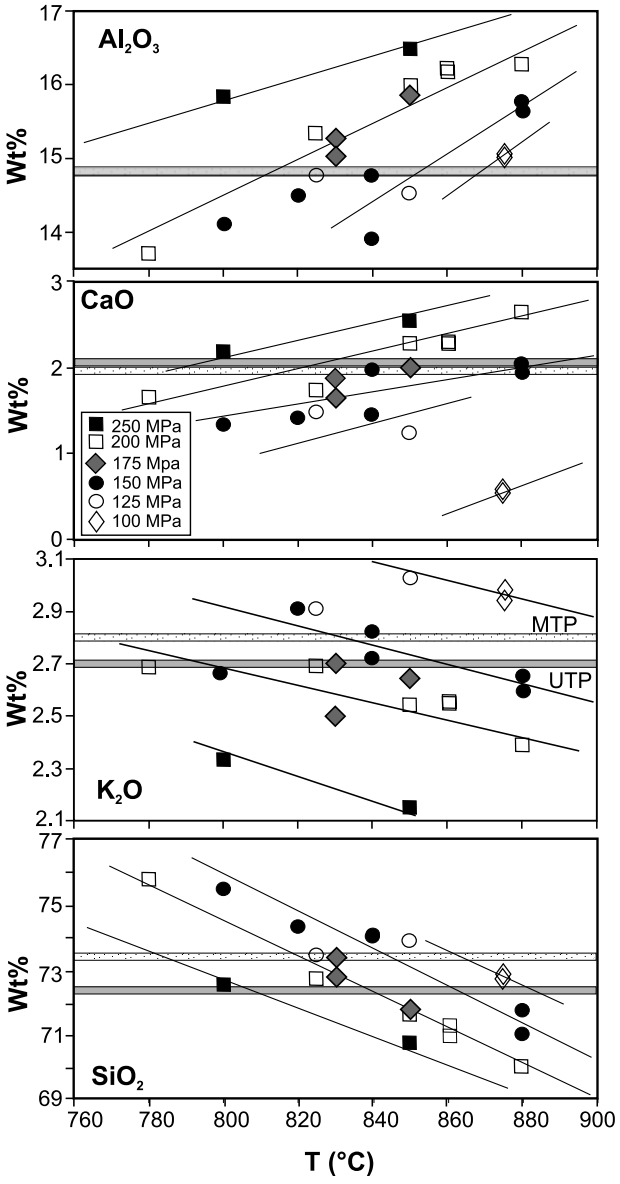

Fig. 9. Variation of experimental glass compositions as a function of pressure and temperature. Continuous lines represent isobaric curves. Horizontal lines represent the glass composition in the UTP (grey) and MTP (stippled) natural samples.

systematically in composition as a function of pressure and temperature (Fig. 9). With decreasing temperature at constant pressure, SiO_2, Na_2O, and K_2O contents increase, whereas those of Al_2O_3, FeO*, MgO, and CaO decrease. With decreasing pressure at constant temperature, SiO_2, Na_2O, and K_2O contents increase, whereas those of Al_2O_3, FeO*, MgO, and CaO decrease. These variations are expected, given that decreasing temperature and pressure trigger crystallization of plagioclase + orthopyroxene (±hornblende) + Fe–Ti oxides.

DISCUSSION

Pre-eruptive conditions of the Nevado de Toluca magmas

Assuming that biotite is xenocrystic, the stable phase assemblage in the three Toluca magmas is rhyolitic melt (glass) + plagioclase + hornblende + orthopyroxene + Fe–Ti oxides. For the UTP magma at ~824°C, those five phases occur together at water pressures >150 MPa (Fig. 8). When comparing natural and experimental glasses, we find that there is reasonably good agreement at pressures between 150 and 200 MPa (Fig. 9).

We did not perform experiments on MTP samples, but their bulk compositions are similar enough to the UTP pumice (Table 7) that it is unlikely that the results would be different. Again, assuming that biotite is xenocrystic, the similarities in glass composition and phase compositions to UTP samples, and the only slightly lower temperature, suggest that there was little difference in water pressures between the MTP and UTP magmas. We lack compositional data for matrix glass in BAF-13, but its similar phase assemblage and bulk composition to the MTP and UTP samples suggest that its storage conditions were also similar to those for the other magmas. These results imply that all three Toluca magmas were stored at similar conditions, which would have been ~4·5–6 km depth (Fig. 10), assuming the magma was water saturated.

Evolution of the Toluca magma chamber from 13 to 10·5 ka

The three eruptions represent a total of ~10–11 km^3 of magma, with BAF-13 constituting ~0·5 km^3 of magma, MTP ~1·8 km^3, and UTP ~8 km^3. All three magmas have similar whole-rock compositions, mineral assemblages, mineral compositions and pre-eruptive conditions, and contain biotite xenocrysts. There are two possibilities to explain how the plumbing system could have produced compositionally identical magmas over 2500 years of activity. First, each erupted magma could have been generated separately, by partial melting of the lower crust as attested by crustal xenoliths found in the area (Martínez-Serrano *et al.*, 2004; Meriggi *et al.*, 2004), and then ascended and erupted. This would require that each partial melting event occurred to essentially the same extent each time, involved the same crustal substrate, and that the resultant magma ascended to the same shallow level before erupting. The other possibility is that each eruption tapped the same magma body, and that the magma body did not evolve significantly for ~2500 years. Although we cannot rule out the first hypothesis, we believe that the second is more likely, given that each magma appears to come from the same

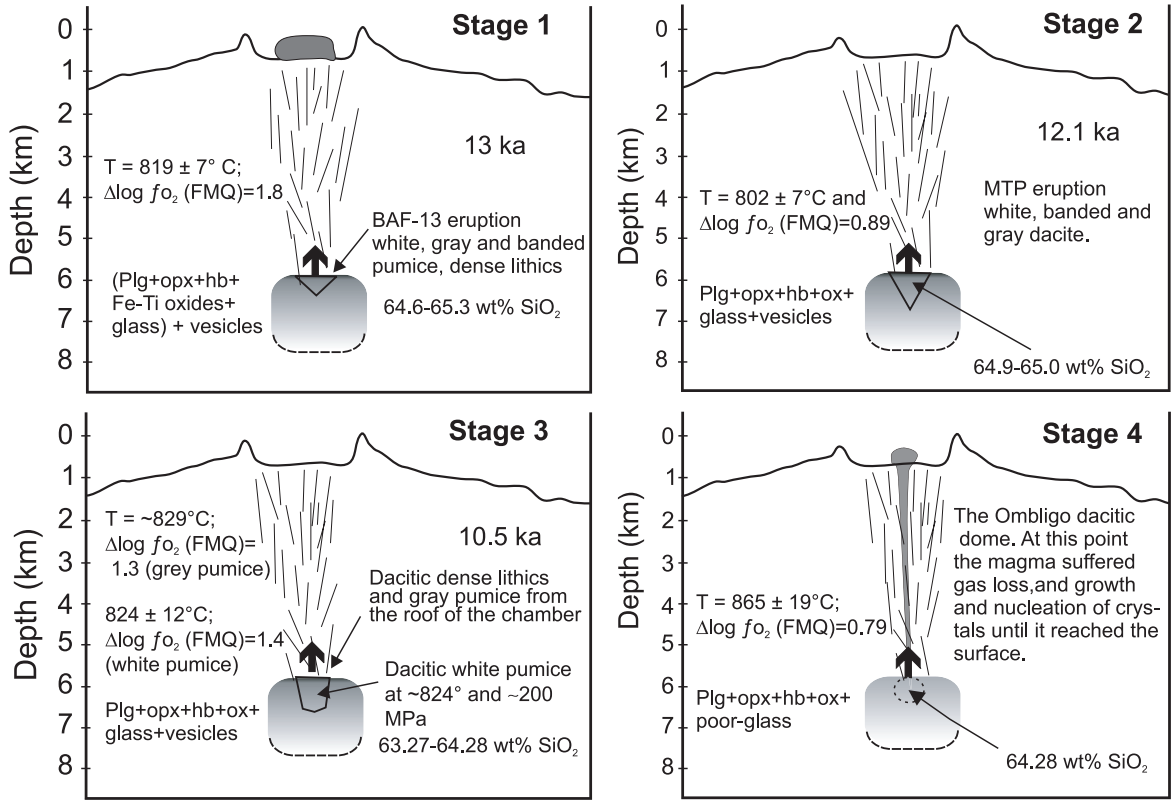

Fig. 10. Schematic model that shows the evolution of the Nevado de Toluca magma system during the last three major eruptions at 13, 12·1, and 10·5 ka.

storage level, at about the same temperature, and that all contain biotite xenocrysts.

Given our hypothesis that the same magma body was tapped three times, minor differences in crystal content and glass composition between the grey and white pumice of the three eruptions could reflect their origin from different levels in the magma storage reservoir. In the case of the UTP samples, the grey pumice is slightly cooler than the white pumice (Table 7), suggesting that the grey pumice could have come from the upper, cooler part of the magma reservoir whereas the white pumice was derived from the main part of the magma body. The stratigraphic section through the UTP (Fig. 2) supports this idea, as grey pumice and dense lithic fragments are abundant at the base of the UTP sequence. The presence of white, grey, and banded pumice suggests that the two levels of the magma body (upper grey and lower white) underwent mechanical mingling during simultaneous tapping (Freundt & Tait, 1986).

Average temperatures of the magmas varied from 802 ± 7 to 824 ± 12°C during the 2500 year eruptive period. This may represent slight warming of the magma reservoir with time, probably by injections of mafic magma at the base of the chamber. The observed disequilibrium textures of the large phenocrysts may originate from such injections. These injections would have to be large enough to significantly raise the temperature (to cause resorption), but the magma body would then have to cool to almost the original temperature, for microphenocrysts to grow under the same conditions as the phenocrysts. Instead of such fluctuations in temperature, however, we believe that the slight variations in temperature may simply reflect the tapping of different levels in the reservoir, similar to the model proposed for the white vs grey pumice. This would also fit the trend of generally hotter magmas being erupted in larger volumes.

Changes in the magma reservoir must have occurred with time; we note that the oxygen fugacity of the magma lowered by one unit of Δlog FMQ with time between BAF-13 and MTP, and a little higher for the UTP. This change may have occurred as a consequence of wall-rock assimilation.

Based on Sr, Nd, and Pb isotopic data, Martínez-Serrano *et al.* (2004) concluded that all the dacitic rocks of Nevado de Toluca have been produced by fractional crystallization and minor crustal contamination. However, our data indicate that crustal assimilation may have played an important role in the evolution of the magmatic system of Nevado de Toluca to produce dacitic magmas. Assimilation of relatively young plutonic bodies (e.g. >4 Ma), with similar whole-rock compositions to those of the Toluca magmas, could have occurred. This

has been observed in other volcanic systems and called 'cryptic' assimilation (Reagan *et al.*, 2003). This process can be difficult to detect, even with isotopic data such as those reported by Martínez-Serrano *et al.* (2004) for the Nevado de Toluca rocks. We propose that the dacites produced by the three eruptions were generated by combined 'cryptic' assimilation and crystal fractionation.

CONCLUSIONS

After 11·5 ka of quiescence the Nevado de Toluca volcano started a new period of explosive activity between 13 ka and 10·5 ka. During this time ~10 km^3 of dacitic magma was ejected in three episodes. The products have similar whole-rock compositions (63·3–65·7 wt % SiO_2) and mineral assemblages (Plg > Opx > Hb ≫ biotite xenocrysts ≫ Fe–Ti oxides). One of the most interesting aspects of these rocks is the common presence of biotite with reaction rims, as well as the presence of mineral phases with resorbed margins. Based on $^{40}Ar/^{39}Ar$ analyses of single biotite crystals, we believe they are xenocrysts. Thus, we show that although the magmas were similar in composition, assimilation of biotite-bearing wall-rocks with a minimum $^{40}Ar/^{39}Ar$ age of 4 Ma must have occurred throughout the 2500 years of activity. To maintain a near-constant temperature and composition of the magmas we propose that the dacitic reservoir was reheated by small batches of hotter magma. The magma that fed the three eruptions was stored at 150–200 MPa and was probably thermally zoned.

ACKNOWLEDGEMENTS

This research was partially supported by CONACyT grants (27993-T and 38586-T to J.L.M.), National Science Foundation grant (EAR-0229290 to J.G.) and a GSA 'Lipman Research Fund' (to J.L.A.). We are indebted to J. M. Espíndola, C. Siebe, J. C. Mora, and L. Capra for the constructive discussion of the ideas presented in this work. Thanks go to B. Brown, who performed the microprobe analyses of biotite xenocrysts. We are indebted to M. Dungan, B. Singer, S. Nelson, R. Frost (Editor) and M. Wilson (Executive Editor) for their careful reviews of the manuscript.

REFERENCES

Andersen, D. J., Lindsley, D. H. & Davidson, P. M. (1993). QUILF: a PASCAL program to assess equilibria among Fe–Mg–Ti oxides, pyroxenes, olivine, and quartz. *Computers in Geosciences* **19**, 1333–1350.

Arce, J. L., Macías J. L. & Vázquez-Selem, L. (2003). The 10·5 ka Plinian eruption of Nevado de Toluca volcano, Mexico: stratigraphy and hazard implications. *Geological Society of America Bulletin* **115**, 230–248.

Arce, J. L., Cervantes, K. E., Macías, J. L., and Mora, J. C. (2005) The 12.1 ka Middle Toluca Pumice: A dacitic Plinian-subplinian eruption of Nevado de Toluca volcano in Central Mexico. *Journal of Volcanology and Geothermal Research* **147**, 125–143.

Berman, R. G. (1981). Differentiation of calc-alkaline magmas: evidence from the Coquihalla volcanic complex, British Columbia. *Journal of Volcanology and Geothermal Research* **9**, 151–179.

Bloomfield, K. & Valastro, S. (1974). Late Pleistocene eruptive history of Nevado de Toluca Volcano, Central Mexico. *Geological Society of America Bulletin* **85**, 901–906.

Bloomfield, K., Sánchez-Rubio, G. & Wilson, L. (1977) Plinian eruptions of Nevado de Toluca. *Geologische Rundschau* **66**(1), 120–146.

Caballero-Miranda, M., Macías, J. L., Lozano-García, M. S. & Urrutia-Fucugauchi, J. (2001). Late Pleistocene–Holocene volcanic stratigraphy and palaeoenvironments of the Upper Lerma Basin, Mexico. *Sedimentology* **30**, 247–261.

Campa, M. F., Campos, M., Flores, R. & Oviedo, R. (1974). La secuencia mesozoica volcano-sedimentaria metamorfizada de Ixtapan de la Sal, México–Teloloapan, Guerrero. *Boletín de la Sociedad Geológica Mexicana* **35**, 7–28.

Cantagrel, J. M., Robin, C. & Vincent, P. (1981). Les grandes atapés d'évolution d'un volcan andesitique composite: exemple du Nevado de Toluca. *Bulletin of Volcanology* **44**, 177–188.

Carmichael, I. S. E. (1991). The redox states of basic and silicic magmas: a reflection of their source regions? *Contributions to Mineralogy and Petrology* **106**, 129–141.

Cervantes, K. (2001). La Pómez Blanca Intermedia: depósito producido por una erupción pliniana–subpliniana del Volcán Nevado de Toluca hace 12,100 años. Masters thesis, Universidad Nacional Autónoma de México, Mexico City. 84 pp.

Chen, Y., Smith, P. E., Evensen, N. M., York, D. & Lajoi, K. R. (1996). The edge of time: dating young volcanic ash layers with the ^{40}Ar–^{39}Ar laser probe. *Science* **274**, 1176–1178.

Costa, F. & Pichavant, M. (2003). Experimental constraints on volatile abundances in arc magmas and their implications for degassing processes. In: Oppenheimer, C., Pyle, D. & Barclay, J. (eds) *Volcanic Degassing. Geological Society, London, Special Publications* **213**, 23–52.

Costa, F., Scaillet, B. & Pichavant, M. (2004). Petrological and experimental constraints on the pre-eruption conditions of Holocene dacite from Volcán San Pedro (36°S, Chilean Andes) and the importance of sulphur in silicic subduction-related magmas. *Journal of Petrology* **45**, 855–881.

De Cserna, Z., Fries, C., Rincon-Orta, C., Silver, L. T., Westley, H., Solorio-Munguia, J. & Schmitter-Villada, E. (1974). Datos geocronométricos terciarios de los Estados de México y Guerrero. *Boletín, Asociación Mexicana de Geólogos Petroleros* **26**, 263–273.

Devine, J. D., Gardner, J. E., Brack, H. P., Layne, G. D. & Rutherford, M. J. (1995). Comparison of microanalytical methods for estimating H_2O contents of silicic volcanic glasses. *American Mineralogist* **80**, 319–328.

Eichelberger, J. C. (1975). Origin of andesite and dacite: evidence of mixing at Glass Mountain in California and other Circum-Pacific volcanoes. *Geological Society of America Bulletin* **86**, 1381–1391.

Fonarev, V. I. & Konilov, A. N. (1986). Experimental study of Fe–Mg distribution between biotite and orthopyroxene at $P = 490$ MPa. *Contributions to Mineralogy and Petrology* **93**, 227–235.

Francis, P. W., Hynes, A. J., Ludden, J. N. & Bedard, J. (1980). Partial melting or fractional crystallization? A compromise in mafic volcanics of the Proterozoic of Ungava, Quebec. *EOS Transactions, American Geophysical Union* **71**, 1155.

Freundt, A. & Tait, S. R. (1986). The entrainment of high-viscosity magma into low-viscosity magma in eruption conduits. *Bulletin of Volcanology* **48**, 325–339.

Frost, B. R. (1991). Magnetic petrology: factors that control the ocurrence of magnetite in crustal rocks. In: Lindsley, D. H. (ed.)

Oxide Minerals: Petrologic and Magnetic Significance. Mineralogical Society of America, Reviews in Mineralogy **25**, 481–509.

García-Palomo, A., Macías, J. L., Arce, J. L., Capra, L., Garduño, V. H. & Espíndola, J. M. (2002). Geology of Nevado de Toluca volcano and surrounding areas, central Mexico. *Geological Society of America Map Series* 1–48.

Gardner, J. E., Rutherford, M., Carey, S. & Sigurdsson, H. (1995). Experimental constraints on pre-eruptive water contents and changing magma storage prior to explosive eruptions of Mount St Helens volcano. *Bulletin of Volcanology* **57**, 1–17.

Gardner, J. E., Layer, P. W. & Rutherford, M. J. (2002). Phenocrysts versus xenocrysts in the youngest Toba Tuff: implications for the petrogenesis of 2800 km^3 of magma. *Geology* **30**, 347–350.

Gerlach, D. C. & Grove, T. L. (1982). Petrology of Medicine Lake Highland volcanics: characterization of end-members of magma mixing. *Contributions to Mineralogy and Petrology* **80**, 147–159.

Geschwind, C. H. & Rutherford, M. J. (1992). Cummingtonite and the evolution of the Mount St. Helens (Washington) magma system: an experimental study. *Geology* **20**, 1011–1014.

Grant, N. K., Rose, W. I. & Fultz, L. A. (1984). Correlated Sr isotope and geochemical variations in basalts and basaltic andesites from Guatemala. In: Harmon, R. S. & Barreiro, B. A. (eds) *Andean Magmatism*. Nantwich: Shiva, pp. 139–149.

Grove, T. L., Donnelly-Nolan, J. M. & Housh, T. B. (1997). Magmatic processes that generated the rhyolite of Glass Mountain, Medicine Lake volcano, N. California. *Contributions to Mineralogy and Petrology* **127**, 205–223.

Halliday, A. N., Mahood, G. A., Holden, P., Metz, J. M., Dempster, D. J. & Davidson, J. P. (1989). Evidence for long residence times of rhyolitic magma in the Long Valley magmatic system: the isotopic record in precaldera lavas of Glass Mountain. *Earth and Planetary Science Letters* **94**, 274–290.

Hammond, P. A. & Taylor, L. A. (1982). The ilmenite/magnetite assemblage: kinetics of re-equilibration. *Earth and Planetary Science Letters* **61**, 143–150.

Harmon, R. S., Thorpe, R. S. & Francis, P. W. (1981). Petrogenesis of Andean andesites from combined Sr–O relationships. *Nature* **290**, 396–399.

Hawkesworth, C. J., Blake, S., Evans, P., Hughes, R., Macdonald, R., Thomas, L. E., Turner, S. & Zellmer, G. (2000). Time scales of crystal fractionation in magma chambers—integrating physical, iso topic and geochemical perspectives. *Journal of Petrology* **41**, 991–1006.

Hopson, C. & Mattinson, J. (1990). Chelan Migmatite Complex; a Cretaceous protodiapiric mash zone in the North Cascades, Washington. *Geological Society of America, Abstracts with Programs* **22**, 29–30.

Huppert, H. E. & Sparks, R. S. J. (1988). The generation of granitic magmas by intrusion of basalt into continental crust. *Journal of Petrology* **29**, 599–624.

Layer, P. W. (2000). Argon-40/argon-39 age of the El'gygytgyn impact event, Chukotka, Russia. *Meteoritics and Planetary Sciences* **35**, 591–599.

Layer, P. W., Hall, C. M. & York, D. (1987). The derivation of $^{40}Ar/^{39}Ar$ age spectra of single grains of hornblende and biotite by laser step-heating. *Geophysical Research Letters* **14**, 757–760.

Le Bas, M. J., Le Maitre, R. W., Streckeisen, A. & Zanettin, B. (1986). A chemical classification of volcanic rocks based on the total alkali–silica diagram. *Journal of Petrology* **27**, 745–750.

Lindsley, D. H., Frost, B. R., Ghiorso, M. S. & Sack, R.O. (1991). Oxides lie: the Bishop Tuff did not erupt from a thermally zoned magma body. *EOS Transactions, American Geophysical Union* **72**, 312.

Lo Bello, P., Féraud, G., Hall, C. M., York, D., Lavina, P. & Bernat, M. (1987). $^{40}Ar/^{39}Ar$ step-heating and laser fusion dating of a Quaternary pumice from Neschers, Massif central, France: the defeat of xenocrystic contamination. *Chemical Geology* **66**, 61–71.

Macías, J. L., Garcia-Palomo, A., Arce, J. L., Siebe, C., Espíndola, J. M., Komorowski, J. C. & Scott, K. M. (1997). Late Pleistocene–Holocene cataclysmic eruptions at Nevado de Toluca and Jocotitlán volcanoes, Central Mexico. In: Kowallis, B. J. (ed.) *Proterozoic to Recent Stratigraphy, Tectonics, and Volcanology, Utah, Nevada, Southern Idaho and Central Mexico, Geological Society of America, Field Trip Series*. Vol. 42, 493–528.

Martínez-Serrano, R. Schaaf, P., Solís-Pichardo, G., Hernández-Bernal, M. S., Hernández-Treviño, T., Morales-Contreras, J. J. & Macías, J. L. (2004). Sr, Nd and Pb isotope and geochemical data from the Quaternary Nevado de Toluca volcano, a source of recent adakitic magmatism, and the Tenango Volcanic Field, Mexico. *Journal of Volcanology and Geothermal Research* **138**, 77–110.

McDougall, I. & Harrison, T. M. (1999). *Geochronology and Thermochronology by the $^{40}Ar/^{39}Ar$ method*, 2nd edn. Oxford: Oxford University Press, 269 pp.

Meriggi, L., Macías, J. L., Tommasini, S. & Vaggelli, G. (2004). GSA Penrose Conference. Evidence of heterogeneous mantle and magmatic evolution processes beneath the western Chichinautzin Volcanic Field, Central Mexico. In: Aguirre-Díaz, G., Macías, J. L. & Siebe, C. (eds) *Neogene–Quaternary Continental Margin Volcanism*, Instituto de Geología, UNAM, Mexico, D.F., 54 pp.

Nelson, S. T., Davidson, J. & Sullivan, K. R. (1992). New age determinations of central Colorado Plateau laccoliths, Utah: recognizing disturbed K–Ar systematics and re-evaluating tectono-magmatic relationships. *Geological Society of America Bulletin* **104**, 1547–1560.

Reagan, M. K., Sims, K. W. W., Erich, J., Thomas, R. B., Cheng, H., Edwards, R. L., Layne, G. & Ball, L. (2003). Time-scales of differentiation from mafic parents to rhyolite in North American continental arcs. *Journal of Petrology* **44**, 1703–1726.

Reid, F. W. & Cole, J. W. (1983). Origin of dacites of the Taupo volcanic zone, New Zealand. *Journal of Volcanology and Geothermal Research* **18**, 191–214.

Rutherford, M. J. & Hill, P. M. (1993). Magma ascent rates from amphibole breakdown: an experimental study applied to the 1980–1986 Mount St. Helens eruptions. *Journal of Geophysical Research* **98**, 19667–19685.

Singer, B. S., Wijbrans, J. R., Nelson, S. T., Pringle, M. S., Feeley, T. C. & Dungan, M. A. (1998). Inherited argon in a Pleistocene andesite lava: $^{40}Ar/^{39}Ar$ incremental-heating and laser-fusion analyses of plagioclase. *Geology* **26**, 427–430.

Sparks, R. S. J., Huppert, H. E., Wilson, C. J. N., Halliday, A. N. & Mahood, G. A. (1990). Evidence for long residence times of rhyolitic magma in the Long Valley magmatic system; the isotopic record in precaldera lavas of Glass Mountain; discussion and replies. *Earth and Planetary Science Letters* **99**, 387–399.

Spell, T. L., Smith, E. I., Sanford, A. & Zanetti, K. A. (2001). Systematics of xenocrystic contamination: preservation of discrete feldspar populations at McCullough Pass Caldera revealed by $^{40}Ar/^{39}Ar$ dating. *Earth and Planetary Science Letters* **190**, 153–165.

Steiger, R. H. & Jäger, E. (1977). Subcommission on geochronology: convention on the use of decay constants in geo- and cosmochronology. *Earth and Planetary Science Letters* **36**, 359–362.

van den Bogaard, P. & Schirnick, C. (1995). $^{40}Ar/^{39}Ar$ laser probe ages of Bishop Tuff quartz phenocrysts substantiate long-lived silicic magma chamber at Long Valley, United States. *Geology* **23**, 759–762.

Venezky, D. Y. & Rutherford, M. J. (1999). Petrology and Fe–Ti oxide reequilibration of the 1991 Mount Unzen mixed magma. *Journal of Volcanology and Geothermal Research* **89**, 213–230.

York, D., Hall, C. M., Yanase, Y., Hanes, J. A. & Kenyon, W. J. (1981). $^{40}Ar/^{39}Ar$ dating of terrestrial minerals with a continuous laser. *Geophysical Research Letters* **8**, 1136–1138.

APPENDIX A: METHODS

Whole-rock analysis

A total of nine whole-rock chemical analyses were carried out on samples of the three deposits, in addition to 12 analyses (Table 7) that have been reported in the literature (Macías *et al.*, 1997; Arce *et al.*, 2003). Each analysis was made on individual pumice fragments by fusion-inductively coupled plasma emission spectrometry (F-ICPES) at Activation Laboratories, Ancaster, Canada. For the MTP and BAF-13 deposits, white and grey pumice were analyzed and for the UPT deposit we analyzed white and grey pumice, as well as dense, juvenile, lithic clasts and the central dome. In this paper, we report only major element data.

Modal analysis

The modal mineralogy was determined for seven representative samples of the deposits (Table 1). Two samples were analyzed for the BAF-13 deposit: a white pumice (264-wp-f), and a grey pumice (264-gp-f). Two samples were analysed for the MTP deposit: a white pumice (PBI-2A), and a grey pumice (PBI-29B). Three samples were analysed for the UTP deposit: a white pumice (PC2b), a grey pumice (PC0g), and the Ombligo central dome (9596). For each sample, we counted a minimum of 525 and a maximum of 1500 points, consisting of phenocrysts, groundmass (glass + microlites), and vesicles.

Electron microprobe

Microprobe analyses of mineral phases and glasses were performed at the University of Alaska Fairbanks, using a CAMECA SX-50 microprobe with four wavelength-dispersive spectrometers. A total of fifteen experimental samples (listed in Table 9), and eight natural samples from the deposits (Table 2) were analyzed: PC2A, PC1b, PC3, PC0g, and 9596 for the UTP; PBI-29b and PBI-2A for the MTP; 264 for the BAF-13. The analysis of the mineral phases was carried out with a focused beam, an accelerating voltage of 15 keV, and a beam current of 15 nA. For the glass analyses, a 10 μm defocused beam was used, with an accelerating voltage of 15 keV, and a

Table 9: Glass composition in selected experimental runs determined by electron microprobe analysis

Experiment	SiO_2	TiO_2	Al_2O_3	FeO*	Mn	MgO	CaO	Na_2O	K_2O	Cl	Total	*n*
G-244B	71·63	0·26	15·98	2·23	n.d.	0·69	2·28	4·32	2·54	0·06	100	9
G-241	75·80	0·18	13·72	1·36	n.d.	0·24	1·66	4·30	2·69	0·06	100	4
G-247B	69·99	0·38	16·26	2·62	n.d.	1·01	2·65	4·64	2·39	0·06	100	7
G-256	72·71	0·21	15·34	2·11	n.d.	0·59	1·75	4·44	2·69	0·18	100	5
G-257B	73·89	0·17	14·54	2·04	n.d.	0·56	1·24	4·43	3·03	0·12	100	7
G-258B	73·45	0·24	14·76	2·07	n.d.	0·58	1·48	4·39	2·91	0·12	100	8
G-272A	74·08	0·23	14·77	1·66	n.d.	0·42	1·45	4·57	2·72	0·10	100	11
G-272B	74·06	0·26	13·91	1·94	n.d.	0·32	1·99	4·50	2·82	0·21	100	9
G-273	74·28	0·15	14·48	2·01	0·02	0·43	1·42	4·30	2·91	n.d.	100	6
G-294	71·73	0·22	15·85	2·39	0·07	0·71	2·01	4·39	2·64	n.d.	100	6
G-295B	72·53	0·28	15·83	1·75	n.d.	0·56	2·19	4·47	2·33	n.d.	100	4
G-302A	72·73	0·30	15·03	2·47	n.d.	0·56	0·56	4·51	2·94	n.d.	100	5
G-302B	72·81	0·27	15·05	2·42	n.d.	0·56	0·56	4·51	2·98	n.d.	100	4
G-333	75·46	0·17	14·11	1·61	0·05	0·39	1·34	4·20	2·66	n.d.	100	3
G-334A	70·74	0·26	16·47	2·25	0·08	0·70	2·55	4·81	2·15	n.d.	100	4
G-336A	71·00	0·36	15·75	2·62	0·07	0·73	2·04	4·78	2·65	n.d.	100	5
G-336B	71·74	0·29	15·66	2·56	0·09	0·66	1·96	4·46	2·59	n.d.	100	2
G-362A	73·34	0·24	15·03	1·83	0·11	0·64	1·88	4·44	2·50	n.d.	100	6
G-362B	72·76	0·29	15·28	2·04	0·05	0·71	1·66	4·52	2·70	n.d.	100	6
G-363A	70·96	0·37	16·22	2·07	0·05	0·90	2·30	4·58	2·54	n.d.	100	6
G-363B	71·22	0·32	16·17	2·15	0·07	0·89	2·27	4·37	2·55	n.d.	100	6
PC2A	72·33	0·24	14·74	2·13	0·04	0·45	2·13	5·00	2·69	0·04	99·80	3

See Table 8 for experimental conditions. Oxides are reported in wt %. Values are average of *n* analyses; n.d., not determined. PC2A is natural sample.
*Total Fe given as FeO.

beam current of 10 nA. Hydrous glasses (experimental samples) were analyzed using the Na-loss routine described by Devine *et al.* (1995).

$^{40}Ar/^{39}Ar$ analysis

Biotite phenocrysts (2 mm in size) were separated from two samples (MTP-45c and MTP-3I) and were analyzed by the $^{40}Ar/^{39}Ar$ method. The biotite separates were wrapped in aluminum foil and loaded into aluminum cans of 2·5 cm diameter and 6 cm height for irradiation at the McMaster Nuclear Reactor along with the standard mineral TCR-2 sanidine with an age of 27·87 Ma (M. Lanphere, personal communication, 2000). Upon their return from the reactor, the individual biotite grains and sanidine monitor minerals were loaded into 2 mm diameter holes in a copper tray that was then loaded in an ultrahigh-vacuum extraction line. The monitors were fused, and samples heated, using a 6 W argon-ion laser following the technique described by York *et al.* (1981), Layer *et al.* (1987) and Layer (2000).

Fifteen separate analyses were performed for each sample, each consisting of a single biotite crystal, which was step heated in 4–9 steps (fractions). Argon purification was achieved using a liquid nitrogen cold trap and a SAES Zr–Al getter at 400C. The samples were analyzed in a VG-3600 mass spectrometer at the Geophysical Institute, University of Alaska Fairbanks. The argon isotopes measured were corrected for system blank and mass discrimination, as well as calcium, potassium and chlorine interference reactions following procedures outlined by McDougall & Harrison (1999) and calculated using the constants of Steiger & Jaeger (1977). System blanks generally were 2×10^{-16} mol ^{40}Ar and 2×10^{-18} mol ^{36}Ar, which are 10–50 times smaller than fraction volumes. Mass discrimination was monitored by running both calibrated air shots and a zero-age glass sample. These measurements were made on a weekly to monthly basis to check for changes in mass discrimination.

Experimental methods

Powdered white pumice from the UTP deposit was used as starting material in all hydrothermal experiments. Each experiment consisted of 30–150 mg of powder plus distilled water, weighed into a $Ag_{70}Pd_{30}$ tube of 2 or 5 mm diameter. Enough water was added so that an excess fluid vapor was present at run conditions to ensure the sample was water-saturated, and hence water pressure equals total pressure. After weighing in the powder and water, the tube was weighed, welded shut with an oxyacetylene torch, and then weighed again to ensure that no water was lost.

All experiments were run in René-style cold-seal pressure vessels. Oxygen fugacity was buffered near NNO + 1 by using a Ni filler rod and water as the pressurizing medium (Geschwind & Rutherford, 1992; Gardner *et al.*, 1995). Temperature and pressure are precise to within ±3°C and ±0·5 MPa, respectively. In three cases, two charges were run together to approach crystal–melt–vapor equilibrium from two directions. The powders used in these reversal experiments were aliquots of previously run experiments (Table 8), chosen so that one charge was a 'melting' experiment, using relatively crystal-rich material, and one charge was a 'crystallization' experiment, using relatively melt-rich material.

APPENDIX B: $^{40}Ar/^{39}Ar$ ANALYTICAL DATA FOR FOUR BIOTITE GRAINS

Details of the $^{40}Ar/^{39}Ar$ analyses (±1σ) of four biotites grains from Toluca samples MTP-31 and MTP-45c

Laser power (mW)	Cumulative ^{39}Ar	$^{40}Ar/^{39}Ar$ measured	±	$^{37}Ar/^{39}Ar$ measured	±	$^{36}Ar/^{39}Ar$ measured	±	% atm. ^{40}Ar	$^{40}Ar^*/^{39}Ar_K$	±	Age (Ma)	± (Ma)
MTP-3I BI#3; weighted average irradiation parameter (J) *from standards = 0·00005997 ± 0·00000039*												
200	0·034	1536·3	288·8	0·404	0·399	5·265	1·004	101·3	−19·67	51·35	−2·13	5·56
400	0·173	1722·8	117·6	0·058	0·108	5·899	0·435	101·2	−20·27	74·54	−2·20	8·07
410	0·220	1346·4	147·2	−0·342	0·259	4·646	0·516	102·0	−26·49	27·98	−2·87	3·03
600	0·326	1562·2	75·6	0·057	0·127	5·290	0·264	100·1	−0·90	23·84	−0·10	2·58
610	0·369	1257·6	151·1	0·187	0·282	4·178	0·509	98·2	22·94	26·23	2·48	2·83
900	0·453	1326·0	108·6	0·096	0·129	4·382	0·371	97·7	30·96	28·12	3·35	3·04
1200	0·537	1383·5	78·4	0·147	0·160	4·653	0·269	99·4	8·46	16·93	0·91	1·83
2000	0·760	1464·8	33·2	0·022	0·058	4·920	0·114	99·3	10·75	11·45	1·16	1·24
8700	1·000	1287·5	31·1	0·135	0·082	4·209	0·102	96·6	43·83	9·81	4·74	1·06
Integrated		1437·6	26·7	0·077	0·042	4·823	0·094	99·1	12·40	11·78	1·34	1·27

Laser power (mW)	Cumulative ^{39}Ar	$^{40}Ar/^{39}Ar$ measured	±	$^{37}Ar/^{39}Ar$ measured	±	$^{36}Ar/^{39}Ar$ measured	±	% atm. ^{40}Ar	$^{40}Ar^*/^{39}Ar_K$	±	Age (Ma)	± (Ma)
MTP-3I BI#5; weighted average irradiation parameter (J) *from standards = 0·00005997 ± 0·00000039*												
200	0·072	1664·2	49·7	−0·009	0·089	5·631	0·175	100·0	0·30		24·68	0·03	2·67
400	0·303	1222·8	28·0	0·130	0·025	4·165	0·086	100·7	−8·10		24·97	−0·88	2·70
600	0·460	1151·1	20·7	0·021	0·054	3·920	0·078	100·6	−7·33		19·56	−0·79	2·12
900	0·563	988·8	22·4	0·027	0·056	3·306	0·083	98·8	11·82		11·76	1·28	1·27
1200	0·661	992·9	21·1	−0·049	0·062	3·261	0·073	97·1	29·19		7·04	3·16	0·76
1800	0·839	858·0	9·4	−0·048	0·040	2·831	0·040	97·5	21·30		8·89	2·30	0·96
2400	0·924	617·7	15·5	−0·012	0·074	2·046	0·059	97·9	12·98		9·03	1·40	0·98
8700	1·000	813·2	24·2	0·020	0·091	2·652	0·090	96·4	29·47		13·15	3·19	1·42
Integrated		1049·1	8·8	0·023	0·019	3·522	0·030	99·2	8·21		7·20	0·89	0·78
MTP-3I BI#10; weighted average irradiation parameter (J) *from standards = 0·00005997 ± 0·00000039*												
200	0·045	1962·9	130·3	−0·334	0·255	6·566	0·442	98·9	22·55		25·14	2·44	2·72
400	0·276	1224·9	22·8	0·097	0·043	4·113	0·065	99·2	9·45		23·52	1·02	2·54
600	0·465	1107·4	23·6	−0·044	0·079	3·715	0·078	99·1	9·69		16·67	1·05	1·80
900	0·577	800·3	20·5	−0·068	0·084	2·679	0·070	98·9	8·49		8·13	0·92	0·88
1200	0·697	720·7	18·2	−0·013	0·097	2·457	0·066	100·7	−5·36		9·23	−0·58	1·00
1800	0·844	674·8	12·2	−0·069	0·079	2·250	0·043	98·5	9·83		7·68	1·06	0·83
2400	0·914	799·4	30·8	−0·100	0·164	2·655	0·107	98·1	14·82		10·01	1·60	1·08
8900	1·000	883·5	26·5	−0·044	0·112	2·943	0·091	98·4	13·99		8·21	1·51	0·89
Integrated		987·6	9·3	−0·031	0·032	3·312	0·030	99·1	9·01		6·72	0·97	0·73
MTP-45c BI#11; weighted average irradiation parameter (J) *from standards = 0·00005997 ± 0·00000039*												
200	0·014	640·1	46·5	0·107	0·232	2·187	0·166	101·0	−6·16		17·81	−0·67	1·93
400	0·042	804·0	63·1	0·245	0·144	2·816	0·207	103·5	−28·09		53·67	−3·04	5·82
600	0·079	416·7	24·4	0·156	0·127	1·469	0·098	104·2	−17·35		27·45	−1·88	2·97
900	0·134	217·7	8·7	0·122	0·063	0·757	0·039	102·8	−6·13		8·20	−0·66	0·89
1200	0·204	159·2	3·7	0·081	0·042	0·529	0·019	98·3	2·73		4·86	0·30	0·53
1800	0·373	114·1	1·8	0·053	0·026	0·367	0·010	95·1	5·64		2·88	0·61	0·31
2400	0·665	58·5	2·2	0·036	0·012	0·174	0·009	88·2	6·92		2·43	0·75	0·26
8900	1·000	24·6	0·3	0·026	0·010	0·052	0·003	63·0	9·09		0·97	0·98	0·11
Integrated		114·5	1·8	0·054	0·011	0·373	0·007	96·2	4·35		2·13	0·47	0·23